Cell Reports

Article

CD300f immune receptor contributes to healthy aging by regulating inflammaging, metabolism, and cognitive decline

Graphical abstract

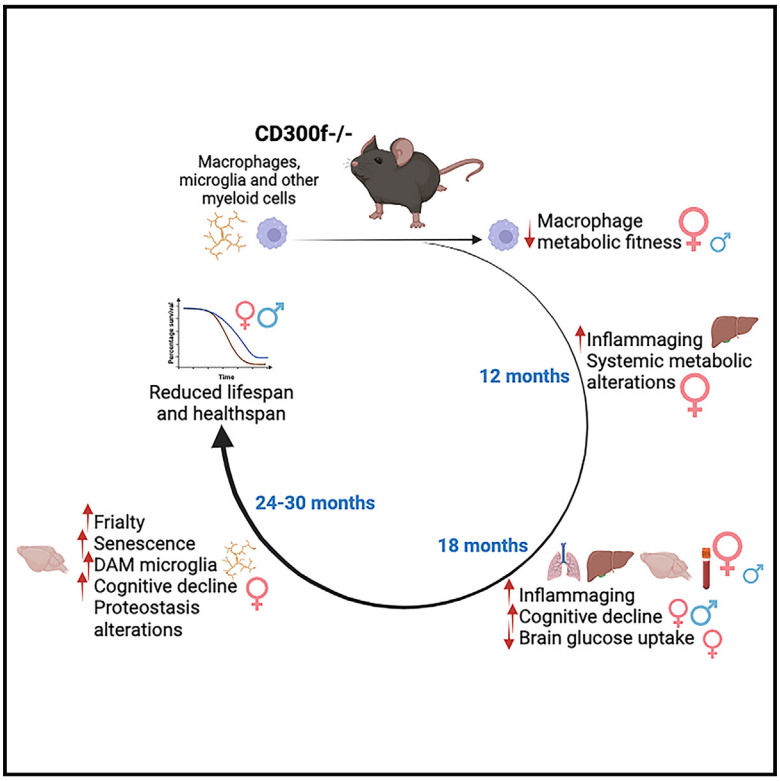

Highlights

- CD300f$^{-/-}$ mice show reduced lifespan, but no specific cause of death is identified
- This is associated with inflammaging, senescence, frailty, and cognitive decline
- CD300f$^{-/-}$ mice exhibit microglial aging states and sex-dependent metabolic changes
- Absence of CD300f reduces macrophage immunometabolic fitness in a sex-dependent way

Authors

Frances Evans, Daniela Alí-Ruiz, Natalia Rego, ..., Cristina Malagelada, Carlos Escande, Hugo Peluffo

Correspondence

hugo.peluffo@ub.edu

In brief

Evans et al. report that the absence of CD300f myeloid cell immune receptor in male and female mice induces a reduced lifespan. Animals display diverse aged-related conditions such as inflammaging, frailty, cognitive decline, brain senescence markers, microglial aging phenotypes, and reduced macrophage metabolic fitness, as well as sex-dependent metabolic alterations.

Evans et al., 2023, Cell Reports *42*, 113269
October 31, 2023
https://doi.org/10.1016/j.celrep.2023.113269

CellPress

Cell Reports

CellPress
OPEN ACCESS

Article

CD300f immune receptor contributes to healthy aging by regulating inflammaging, metabolism, and cognitive decline

Frances Evans,[1,2] Daniela Alí-Ruiz,[2] Natalia Rego,[3,4] María Luciana Negro-Demontel,[1,2] Natalia Lago,[2] Fabio Andrés Cawen,[2] Bruno Pannunzio,[1,2] Paula Sanchez-Molina,[5] Laura Reyes,[6] Andrea Paolino,[6] Jorge Rodríguez-Duarte,[7] Valentina Pérez-Torrado,[8] Almudena Chicote-González,[9,10] Celia Quijano,[11] Inés Marmisolle,[11] Ana Paula Mulet,[12] Geraldine Schlapp,[12] María Noel Meikle,[12] Mariana Bresque,[8] Martina Crispo,[12] Eduardo Savio,[6] Cristina Malagelada,[9,10] Carlos Escande,[8] and Hugo Peluffo[1,2,9,10,13,*]

[1]Department of Histology and Embryology, Faculty of Medicine, UDELAR, Montevideo, Uruguay
[2]Neuroinflammation and Gene Therapy Laboratory, Institut Pasteur de Montevideo, Montevideo, Uruguay
[3]Bioinformatics Unit, Institut Pasteur de Montevideo, Montevideo, Uruguay
[4]Faculty of Sciences, UDELAR, Montevideo, Uruguay
[5]Department of Cell Biology, Physiology and Immunology, and Institute of Neuroscience, Universitat Autònoma de Barcelona, Barcelona, Spain
[6]Uruguayan Center for Molecular Imaging (CUDIM), Montevideo, Uruguay
[7]Laboratory of Vascular Biology and Drug Development, INDICYO Program, Institut Pasteur Montevideo, Montevideo, Uruguay
[8]Metabolic Diseases and Aging Laboratory, INDICYO Program, Institut Pasteur de Montevideo, Montevideo, Uruguay
[9]Unitat de Bioquímica i Biologia Molecular, Departament de Biomedicina, Facultat de Medicina i Ciencies de la Salut, Universitat de Barcelona (UB), Barcelona, Spain
[10]Institut de Neurociències, Universitat de Barcelona (UB), Barcelona, Spain
[11]Departamento de Bioquímica y Centro de Investigaciones Biomédicas (CEINBIO), Facultad de Medicina, Universidad de la República, Montevideo, Uruguay
[12]Unidad de Biotecnología en Animales de Laboratorio, Institut Pasteur de Montevideo, Montevideo, Uruguay
[13]Lead contact
*Correspondence: hugo.peluffo@ub.edu
https://doi.org/10.1016/j.celrep.2023.113269

SUMMARY

Emerging evidence suggests that immune receptors may participate in many aging-related processes such as energy metabolism, inflammation, and cognitive decline. CD300f, a TREM2-like lipid-sensing immune receptor, is an exceptional receptor as it integrates activating and inhibitory cell-signaling pathways that modulate inflammation, efferocytosis, and microglial metabolic fitness. We hypothesize that CD300f can regulate systemic aging-related processes and ultimately healthy lifespan. We closely followed several cohorts of two strains of CD300f$^{-/-}$ and WT mice of both sexes for 30 months and observed an important reduction in lifespan and healthspan in knockout mice. This was associated with systemic inflammaging, increased cognitive decline, reduced brain glucose uptake observed by ^{18}FDG PET scans, enrichment in microglial aging/neurodegeneration phenotypes, proteostasis alterations, senescence, increased frailty, and sex-dependent systemic metabolic changes. Moreover, the absence of CD300f altered macrophage immunometabolic phenotype. Taken together, we provide strong evidence suggesting that myeloid cell CD300f immune receptor contributes to healthy aging.

INTRODUCTION

Aging is a multifactorial process that includes the lifelong accumulation of molecular damage, leading to age-related frailty, disability, and disease, and eventually death. Macrophages occupy multiple tissue niches and support tissue development, maintain homeostasis, and respond to invading pathogens. However, dysregulation of their functions can promote pathological processes including inflammatory diseases, cancer, fibrosis, and impaired tissue repair, all processes strongly associated with aging.[1,2] Emerging evidence suggests that microglia/macrophage immune receptors are involved in many aging-related processes such as energy metabolism, inflammation, and cognitive decline.[3,4] One canonical example is TREM2 lipid-sensing immune receptor, a key regulator of microglial phenotype strongly related to Alzheimer's disease (AD),[4,5] and also involved in adipose tissue and hepatic metabolism and control of inflammation.[1,6] CD300f is another lipid-sensing immune receptor that shares many properties with TREM2 including most of its ligands (i.e., phospholipids and

lipoproteins, among others), its expression pattern in microglia/macrophages (although CD300f is also present in other myeloid cells), its involvement in the regulation of microglia/macrophage phenotype and metabolic fitness,[7] and participation in phagocytic apoptotic cell clearance and synaptic pruning machinery.[7,8] In addition, due to their lipid-binding capacity, it has been proposed that TREM2, and putatively CD300f, may sense tissue damage by acting as damage-associated molecular pattern (DAMP) receptors.[9] CD300f is an exceptional immune receptor as it triggers activating and inhibitory intracellular cell-signaling pathways,[10,11] and indirectly modulates DAP12/TYROBP.[12] Most studies regarding the function of CD300f have shown that it has a protective and anti-inflammatory profile in mice models of multiple sclerosis,[13] lupus,[8,14] allergy,[15] or acute brain damage.[16] However, CD300f activation potentiated microglial proinflammatory profile when these cultures were stimulated with LPS.[17] Moreover, no changes in major proinflammatory signaling molecules were observed in CD300f$^{-/-}$ microglia *in vivo* after LPS intraperitoneal challenge,[7] suggesting complex roles of this immune receptor in the regulation of inflammation. CD300f is among the most upregulated genes in brain microglia/macrophages after several proinflammatory insults such as intraperitoneal LPS injection[7,18] or spinal cord injury,[19] and its upregulation has been associated to promyelinating microglia after demyelinating stimuli[20] and to the neuroprotective response against Tau pathology.[21] Genetic variants of CD300f have also been shown to be involved in human inflammatory and autoimmune disease susceptibility.[7,22,23] Interestingly, CD300f has also been associated to non-classical inflammatory functions of microglial and potentially CNS barrier-associated macrophages (BAMs), leading to modulation of neuropsychiatric conditions such as major depressive disorder and anxiety.[7,24]

Despite all this evidence implicating CD300f in different conditions associated with aging, no one has explored its role in age-dependent accumulation of tissue damage, age-related frailty, disability, and eventually reduced lifespan. Several additional lines of evidence implicate immune receptors in aging. One interesting report showed that the absence of the SiglecE inhibitory immune receptor shortened mice lifespan and was associated to several aging-related conditions.[3] Most of these immune receptors, including CD300f and TREM2 are upregulated with age.[25] Aging induces microglial and macrophage metabolic alterations that contribute to cognitive decline,[26] and both TREM2 and CD300f have been shown to be essential for maintaining microglial and macrophage metabolic fitness under different neuropathological conditions.[7,27] Moreover, most AD-associated genes are involved in phagocytosis/lysosomal pathways,[4] where these lipid binding immune receptors play a central role. Finally, analysis of genomic non-coding regions in AD also points toward microglia, BAMs, or other tissue-resident macrophages as central players,[28,29] again linking these cell types and their phenotype to age-related conditions. Taken together, the above reports put forward the question of whether immune receptors expressed on myeloid cells, and in particular CD300f, can regulate systemic aging-related processes such as metabolism, inflammation, neurodegeneration, and cognitive decline, and ultimately healthy lifespan.

RESULTS

CD300f regulates mice lifespan

Emerging evidence suggests that immune receptors could influence lifespan and aging-associated processes.[3] To explore this hypothesis, we aged CD300f$^{-/-}$ and wild-type (WT) mice and followed them closely for 30 months. Strikingly, CD300f$^{-/-}$ mice showed an important reduction in lifespan (Figure 1A). This effect was observed in three different cohorts, in two different animal facilities (Figures S1A and S1B), and was independent of sex (Figures S1C and S1D). To confirm this finding, we generated a new CD300f-deficient mouse line (CD300f$^{-/-IPMon}$), which also showed a similar reduction in lifespan (Figure 1B). It has been found that exposure of mice maintained under specific pathogen free (SPF) conditions to multiple mouse pathogens matures their immune system, which more closely resembles that seen in adult humans.[30] Interestingly, the reduced lifespan of CD300f$^{-/-}$ mice was observed both under SPF conditions (Figure S1B) and in a closer to real-life housing/immunologic environment (UDELAR animal facility, see materials and methods and Figure S1A).

Although a decreased lifespan was observed, no alterations were detected during aging between WT and CD300f$^{-/-}$ mice in body weight (Figures 1C and S1E) or in spontaneous locomotor activity (Figure 1D). The most common natural cause of age-related deaths in a wide range of mouse strains is cancer.[31] A similar frequency of neoplasms was observed macroscopically in WT and CD300f$^{-/-}$ mice (Figure 1E). However, we noted that CD300f$^{-/-}$ female mice tended to show increased incidence and size of tumors at the base of the skull reminiscent of pituitary tumors, a common aged-related pathology[31] (Figure S1F). To quantify this, we performed qPCR of several pituitary hormone genes from brain samples. Strongly increased mRNA levels for growth hormone (*hg*) and prolactin (*prl*) were observed in female CD300f$^{-/-}$ mice at age 30 months when compared with adult WT or CD300f$^{-/-}$ mice and aged-matched WT mice (Figure S1G). It has been shown that 18-month-old CD300f$^{-/-}$ mice are prone to develop autoimmune disease and splenomegaly only if stimulated with pristane and apoptotic cells.[8] Accordingly, we could not detect significant differences in spleen weight until age 30 months or in euthanized female (Figure 1F) or male (Figure S1H) mice, although CD300f$^{-/-}$ female mice displayed a strong tendency ($p = 0.077$) to show splenomegaly at 18 months, earlier than aged WT mice. Moreover, some WT and CD300f$^{-/-}$ mice that had to be euthanized due to ethical endpoint criteria showed splenomegaly (Figure 1F). We did not find alterations in most hepatic/renal clinical plasma markers (Table S1) or in many rutinary clinical blood parameters (Table S1). However, CD300f$^{-/-}$ aged females that had to be euthanized showed increased levels of gamma-glutamyl transferase (GGT) (Figure 1G), and elevated plasma levels of this enzyme have been significantly associated with all-cause mortality.[32] We found an important dispersion of the data with aging, a common finding in aging studies that reflect interindividual differences due to chronological age not matching biological age for each subject. For instance, some euthanized animals showed increased plasmatic alanine amino transferase (ALT), suggestive of hepatic damage (Figure 1H), and some showed reduced basal glycemia under *ad libitum* feeding (Figure 1I). In addition, some

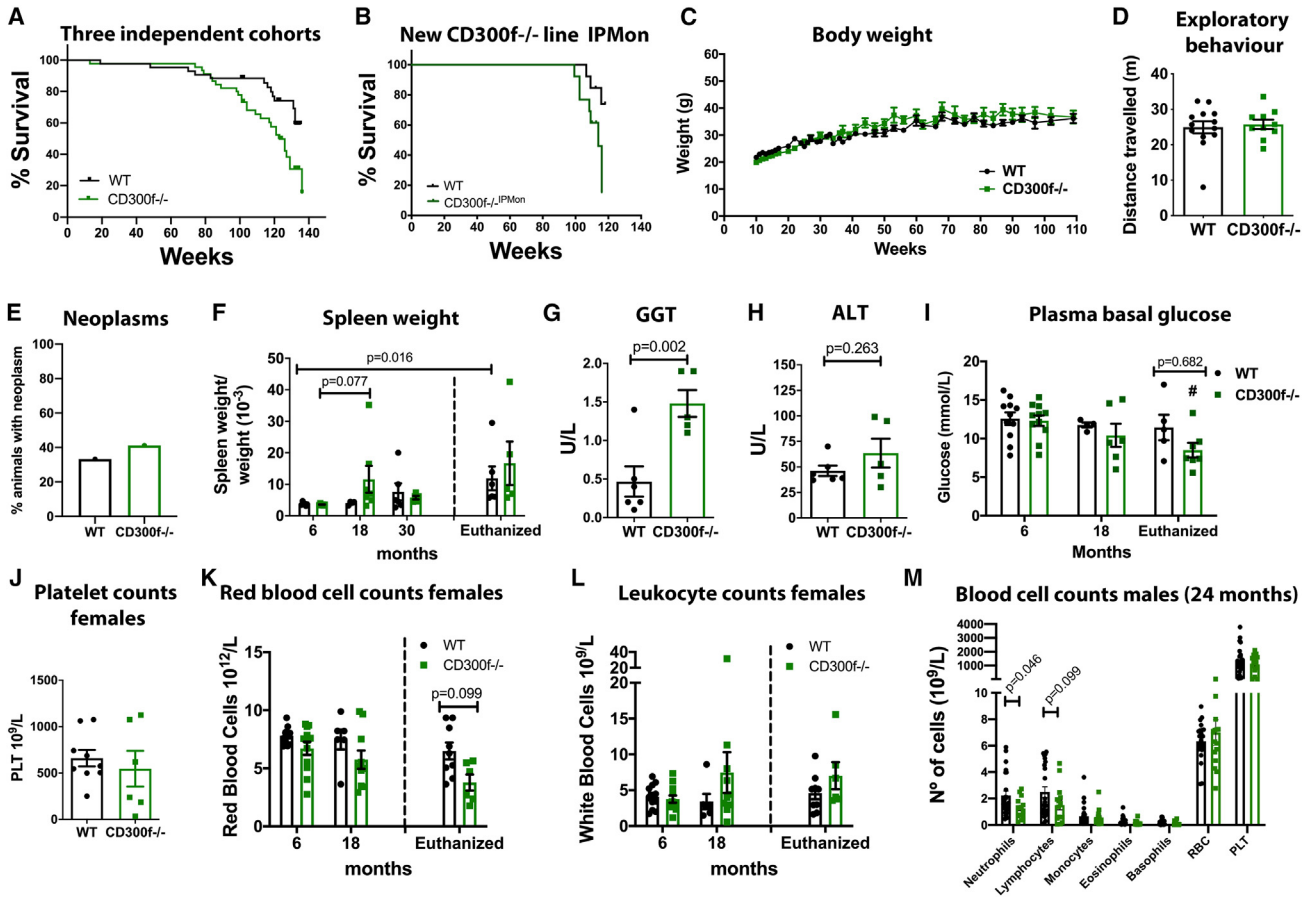

Figure 1. Absence of CD300f reduces lifespan

The lifespan of CD300f$^{-/-}$ and WT animals were followed for 30 months (A) (WT n = 57 and CD300f$^{-/-}$ n = 65, housed at IPMon and UDELAR, log rank Mantel-Cox test, p = 0.0008, median lifespan CD300f$^{-/-}$ 121 weeks) in three independent cohorts (A) and of a new CD300f$^{-/-IPMon}$ line generated (B) (WT n = 13 and CD300f$^{-/-IPMon}$ n = 13 all males, housed in UDELAR, log rank Mantel-Cox test, p = 0.047, median lifespan CD300f$^{-/-}$ 114 weeks). Body weight (males and females) (C). Twenty-five-month-old male and female exploratory behavior in the open field test (D). Percentage of animals with evident neoplasms when euthanized (E) (WT n = 18, CD300f$^{-/-}$ n = 17, lifespan until age 24 months). Relative spleen weight of female mice at the indicated ages (F). Plasma levels of GGT (G) and ALT (H) enzymes, and of platelets (J) in euthanized female mice. Female mice basal glycemia under *ad libitum* feeding at different ages or in female mice that were euthanized (I) (#p = 0.055 and p = 0.090 compared with 6-month-old adult WT or CD300f$^{-/-}$, two-way ANOVA p = 0.049 for age and p = 0.094 for genotype). Blood cell populations in females (K and L) and males (M) (30 months old).

18-month-old and euthanized females showed an important decrease in platelet counts (Figure 1J; Table S1). Also, some 18-month-old and euthanized CD300f$^{-/-}$ females showed anemia (Figure 1K; Table S1) and increased leukocyte counts (Figure 1L; Table S1), while 30-month-old males showed different alterations in white blood cell counts (Figure 1M; Table S1). Taken together, these data show that CD300f$^{-/-}$ mice have a decreased lifespan, and that the underlying cause of death is probably multifactorial and variable depending of the subject, as would be expected for aging.

Absence of CD300f induces inflammaging and systemic metabolic alterations

Chronic low-grade inflammation or inflammaging is a key aspect of aging that contributes to the pathogenesis of age-related diseases.[33] CD300f has been shown to be important to limit the severity of inflammatory conditions by negatively regulating the innate immune system.[10,13,15] To explore the hypothesis that CD300f may contribute to dampen the systemic low-grade inflammation that accumulates during aging, we aged CD300f$^{-/-}$ mice and explored the immune cell infiltration and expression of inflammatory markers in several tissues and plasma. Aging induced widespread inflammaging at 18 months as observed by increased plasma IL-1β, IL-1α, and IL-6 protein levels (Figure 2A) and increased mRNA for *il1β* in lungs (Figure 2B). Cytokines such as TNF-α, INF-β, and INF-γ, among other plasma cytokines measured, did not show significant changes (Figure S2A). Moreover, age-dependent liver accumulation of immune infiltrates in WT animals was observed as described previously (Figures 2C and 2D), a process that was increased in CD300f$^{-/-}$ mice (Figures 2C and 2D). These data are in accordance with the aging-associated accumulation of eosinophils in the adipose tissue at 5–8 months in CD300f$^{-/-}$ mice.[34] The hepatic infiltrates were more pronounced in

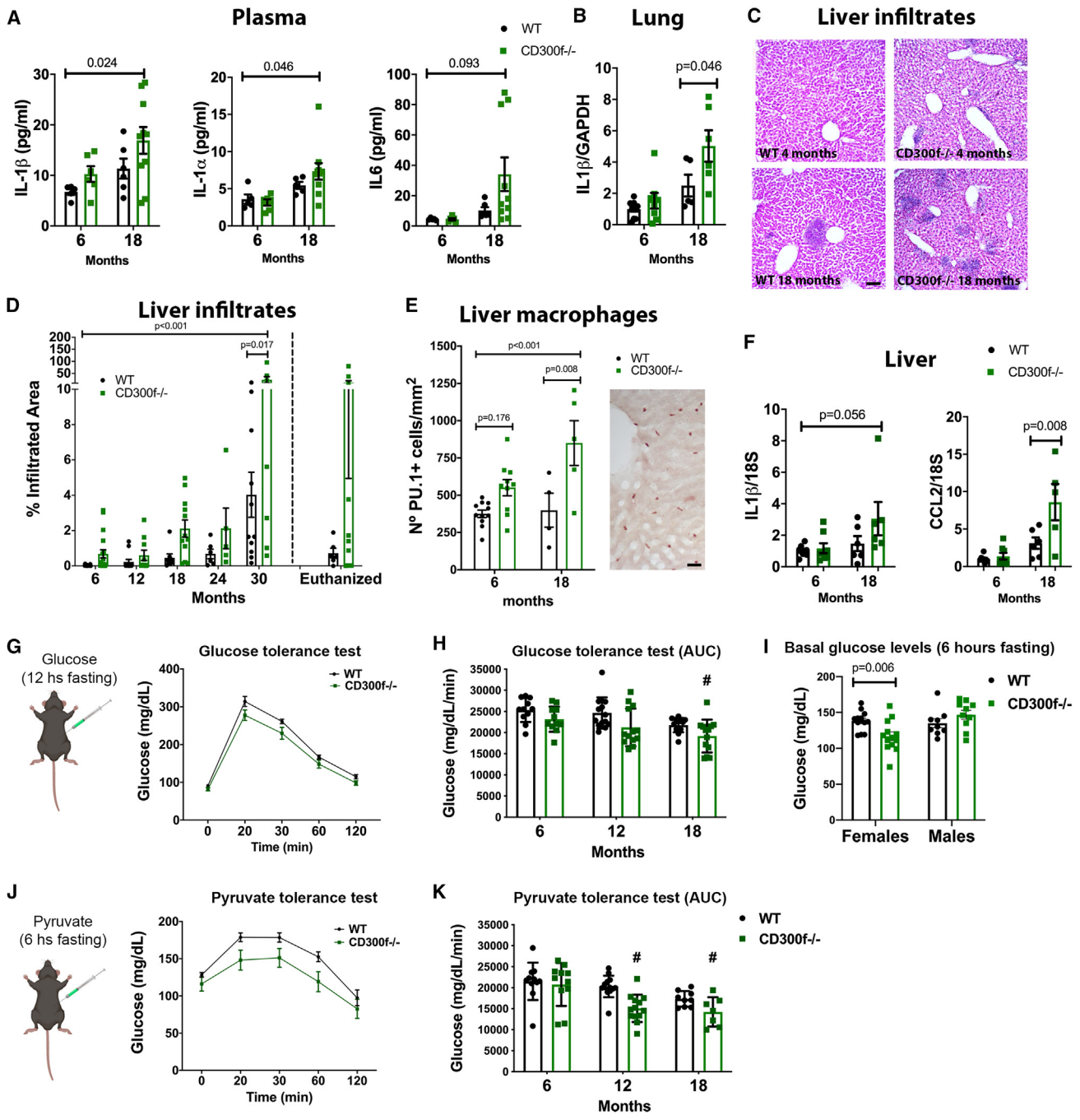

Figure 2. Absence of CD300f induces inflammaging and systemic glucose metabolism alterations

An age-dependent proinflammatory cytokine and chemokine increase in plasma (A) (ELISA), lung (B) (qPCR), and liver (F) (qPCR) was observed in 18-month-old CD300f$^{-/-}$ female mice. Age-dependent hepatic infiltrates were also increased in CD300f$^{-/-}$ mice (male and female pooled data) (C and D). Scale bar, 100 μm. Age-dependent increase in PU.1+ cells in the liver of CD300f$^{-/-}$ mice (females) (E). Scale bar, 50 μm. Glucose tolerance test in adult female mice (G) and at different ages (H) (#p < 0.01 compared with 6- and 12-month-old adult WT, two-way ANOVA p = 0.001 for age and p = 0.001 for genotype) after 12 h fasting. Basal glycemia after 6 h fasting in female and male 18-month-old mice (I). Pyruvate tolerance test in 18-month-old females (J) and at different ages (K) (#p < 0.02 compared with 6- and 12-month-old adult WT, two-way ANOVA p < 0.001 for age and p = 0.002 for genotype) after 6 h fasting. AUC, area under the curve.

CD300f$^{-/-}$ female than male mice, an effect also observed in WT female and male mice (Figures S2B and S2C). The increased liver inflammation in CD300f$^{-/-}$ female mice included increased numbers of PU.1 macrophages (Figure 2E). In accordance, the mRNA for *il1β*, *ccl2* (Figure 2F), and *ccl3* (Figure S2D) were elevated in 18-month-old CD300f$^{-/-}$ female liver. Despite liver

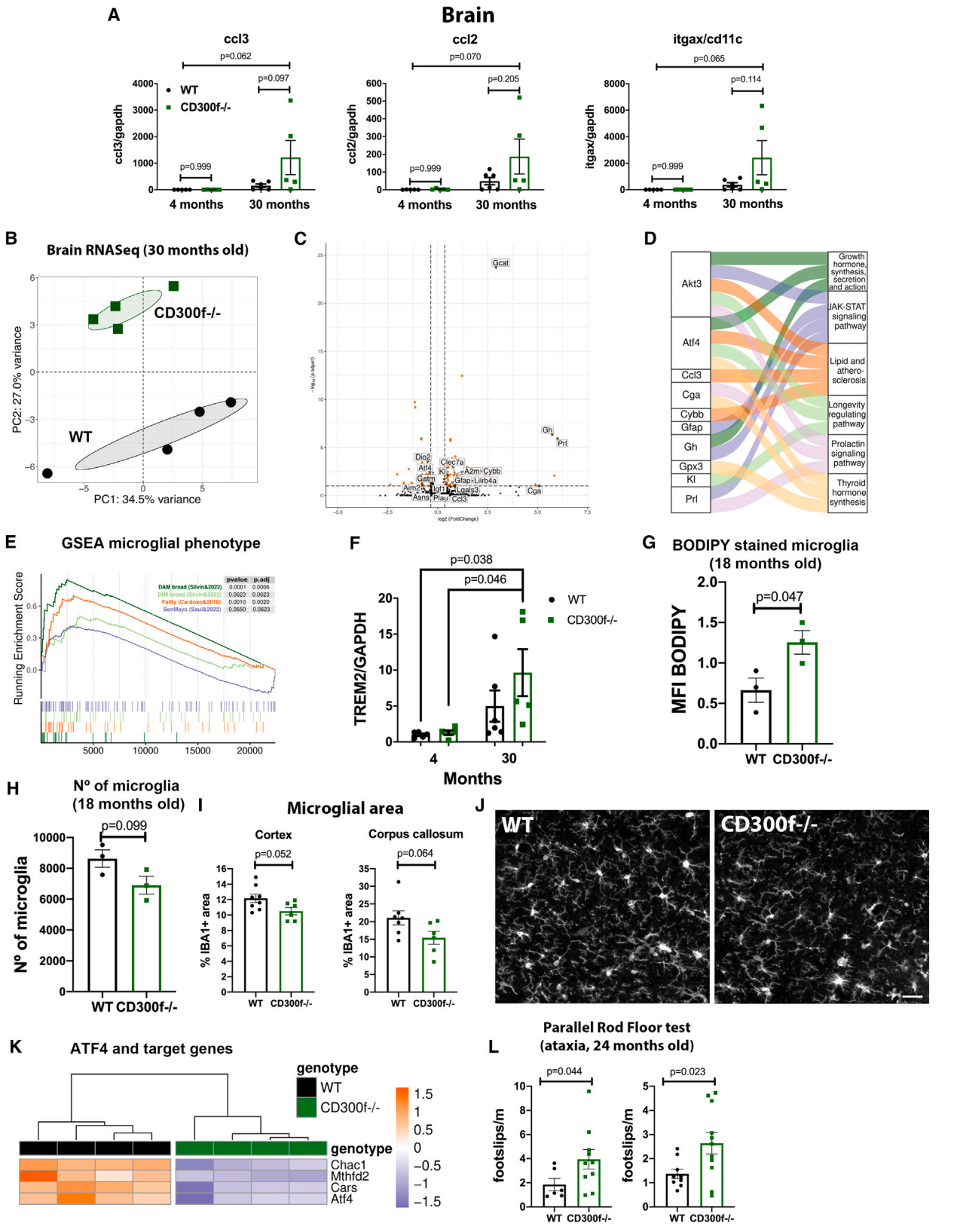

(legend on next page)

inflammation, no general hepatoxicity could be detected by measuring plasma AST and ALT enzymes at 18 and 30 months in most animals (Table S1). Moreover, bone marrow-derived macrophage (BMDM) cultures from adult WT and CD300f$^{-/-}$ female mice showed increased NLRP3 inflammasome expression after LPS stimulation in the latter (Figure S2E), also suggesting increased inflammatory profile of CD300f$^{-/-}$ myeloid cells.

Macrophages and immune receptors such as TREM2 have been shown to regulate both liver and fat tissue metabolism.[1,35] Thus, to explore whether CD300f immune receptor could alter macrophage phenotype and influence systemic metabolism during aging, we explored the age-related alterations in glucose handling and clearing capacity in adult and aged WT and CD300f$^{-/-}$ mice. Adult male and female WT and CD300f$^{-/-}$ mice were able to maintain similar basal plasmatic glucose levels under *ad libitum* feeding and after 6 or 12 h fasting (Figures 2H and 2I), and showed no alteration in glucose buffering capacity as observed after an intraperitoneal glucose challenge (glucose tolerance test [GTT]; and as reported previously[34]) (Figures 2G, 2H, S3A, and S3H). However, 12- and 18-month-old female but not male CD300f$^{-/-}$ mice showed a reduced under the curve area after the GTT, suggesting alterations in glucose-buffering capacity. This effect was not due to differences in insulin sensibility in CD300f$^{-/-}$ mice (mostly due to muscle glucose uptake), as no alterations were observed after an intraperitoneal insulin challenge (insulin tolerance test) in CD300f$^{-/-}$ male and female mice until 18 months, the last age tested (Figures S2F, S2G, and S3I). Interestingly, a short 6-h starvation demonstrated the reduced capacity of 18-month-old CD300f$^{-/-}$ females to sustain basal plasmatic glucose levels (Figure 2I). In this context, the alteration in glucose metabolism could be due to hepatic dysfunction. To test this hypothesis, an intraperitoneal pyruvate injection challenge was performed (pyruvate tolerance test), which mainly evaluates the hepatic gluconeogenesis potential. Interestingly, while WT female mice tend to show a reduced hepatic gluconeogenesis from age 18 months, female, but not male, CD300f$^{-/-}$ mice showed reduced hepatic gluconeogenesis earlier, from age 12 months (Figures 2J, 2K, and S3H).

Absence of CD300f induces age-related CNS alterations

The brain is a central organ affected by aging. Accordingly, signs of inflammaging were also observed in the brain of 30-month-old CD300f$^{-/-}$ mice by qPCR for chemokines *ccl2*, *ccl3*, and *itgax/cd11c* (Figure 3A). To further understand the biological role of CD300f in CNS aging, we analyzed the whole-brain transcriptome by RNA-seq of 30-month-old WT and CD300f$^{-/-}$ female mice (Table S2). The general RNA-seq gene expression profiles of both groups were different, as observed by principal-component analysis (Figure 3B). In fact, 67 genes were significantly differentially expressed (Figure 3C and S4A; Table S3). An over-representation analysis of these genes highlighted an enrichment in KEGG pathways associated to longevity regulation, JAK-STAT and PI3K signaling (Figure 3D; Table S4). These data are in accordance with gene set enrichment analysis (GSEA) of aged microglia that showed increased STAT3 activation.[36] Alteration in the expression of well-known genes related to longevity such as *gh*, *igf1*, *prl*, *kl*, and *gcat* was observed (Figure 3C). For instance, *gcat*, one of the most upregulated genes in CD300f$^{-/-}$ brain, has been shown to be downregulated during normal aging in different species, and knockdown of GCAT increases lifespan in *Caenorhabditis elegans*.[37] This association prompted us to analyze senescence markers in the brain of CD300f$^{-/-}$ mice. A recent report compiled a senescence gene set termed SenMayo, which is able to accurately quantify the degree of senescent cells in RNA-seq samples from several tissues including the brain and microglia of mice and humans.[38] When a GSEA was performed on our RNA-seq data using the SenMayo mouse gene set, a significant enrichment in senescence markers was observed in the CD300f$^{-/-}$ brain (Figure 3E; Table S5). Moreover, GSEA also showed that the brains of 30-month-old CD300f$^{-/-}$ female mice were significantly enriched for disease-associated microglia (DAM)-upregulated genes (including *clec7a*, *ccl3*, *lilrb4*, *cybb*, *lgals3*, and *igf1*) previously observed in aging, AD, and other neurodegenerative conditions[39,40] (Figures 3C and S4B; Table S5). Immunohistochemical analysis for one of the main DAM markers CLEC7A showed a significant increased immunoreactivity in all animals analyzed and increased CLEC7A+ cells only in some animals (Figures S4C–S4E). TREM2 has been shown to be essential for microglial DAM phenotype induction[39] and, in accordance, qPCR showed that TREM2 is upregulated in CD300f$^{-/-}$ 30-month-old aged brains (Figure 3F). A recent study[41] suggests that, among the classical DAM microglia,[39] there is a defined population derived from monocytes termed disease inflammatory macrophages (DIMs) that would accumulate in the brain mainly during aging and neuroinflammation. Interestingly, 30-month-old CD300f$^{-/-}$ mouse brains also showed a significant signature for DIM macrophages (Figures 3E and S4B; Table S5). An additional fact pointing toward an aged microglial phenotype in CD300f$^{-/-}$ 18-month-old brains is the increase in their lipid droplet content (Figure 3G).[42] Microglia have been shown to increase in their number and expression of proinflammatory markers with age.

Figure 3. Absence of CD300f induces age-related brain alterations

Brain inflammatory marker mRNA expression in adult and 30-month-old WT and CD300f$^{-/-}$ female mice was analyzed by qPCR (A). The transcriptome of 30-month-old female brains was analyzed by bulk RNA-seq (B, C, and K). Principal-component analysis (B), volcano plot highlighting differentially expressed genes (C), and KEGG pathway enrichment results (D) of the RNA-seq. The plot depicts the relationships among differentially expressed genes and over represented KEGG pathways ($p < 0.001$, FDR-adjusted p value < 0.2). Gene expression changes in the brain of 30-month-old CD300f$^{-/-}$ compared with WT mice exhibited both frailty and senescent signatures as well as enhanced microglial DAM state and a recruited macrophage DIM profile (E). GSEA plot shows, for the five gene lists, the running enrichment score as well as the position of the specific genes in the ranked gene sorting. qPCR for TREM2 expression in 30-month-old female brains (F). Quantification of microglial BODIPY+ lipid droplet content by flow cytometry in 18-month-old female brains (neocortex) (G). Quantification of microglial numbers by anti-CD11b/CD45 staining and flow cytometry of 18-month-old female brains (neocortex) (H). Quantification of IBA1 staining in 30-month-old female brains by immunohistochemistry (I and J). Scale bar, 20 μm. Normalized expression of ATF4 mRNA and some of its target genes (K) in 30 month-old-female brains. The parallel rod floor test (PRFT) was performed for analyzing ataxia in two independent cohorts of 24-month-old WT and CD300f$^{-/-}$ female mice at two different animal facilities (L). MFI, mean fluorescent intensity.

However, in the aged brains of CD300f$^{-/-}$ female mice, a trend toward displaying reduced numbers of microglia at 18 months (Figure 3H), or in the percentage of the IBA1-stained area at 30 months, was observed (Figures 3I and 3J).

Further exploration of brain RNA-seq results showed that KEGG enrichment analysis also highlighted growth hormone secretion and the action pathway. Indeed, the increase in mRNA for *gh*, *prl*, and *cga* (alpha polypeptide shared by several pituitary hormones) confirmed the previous qPCR data suggesting that CD300f$^{-/-}$ female mice develop pituitary neoplasms. Another differentially expressed gene in 30-month-old CD300f$^{-/-}$ female mice brain was *atf4*, which is a central effector of the integrated stress response. Proteostasis alteration is a hallmark of aging, and upregulation of pathways such as *atf4* have been associated to conditions that extend lifespan.[43] Interestingly, 30-month-old CD300f$^{-/-}$ mice showed decreased mRNA for *atf4* and some of its target genes (Figures 3C and 3K). Finally, the RNA-seq study also detected increased mRNA levels of inflammatory markers related to astrocytes (*gfap*), microglia (*clec7a*), and chemokines (*ccl3*) (Figure 3C). This confirmed whole-brain qPCR analysis of expression of chemokines (*ccl3*) (Figure 3A).

Frailty, another hallmark of aging, is considered an overall measure of unexplained heterogeneity in the accumulation of health-related problems of people of the same chronological age.[44] Interestingly, the frailty indexes have been shown to be similar in mice and people across the life course[45]; they are clinically relevant and predict rodent mortality in a similar manner as clinical frailty indices for humans.[45] The brain of CD300f$^{-/-}$ mice showed a significant enrichment for the frailty markers suggested by Cardoso et al.[46] such as *kl*, *csf1*, *gh*, and *plau* (Figure 3E). Other genes that, although non-significantly differentially expressed, contribute to the frailty running enrichment score in the GSEA were *gpnmb, tgfb1*, *c3*, *c1qa*, *c1qb*, and *c1qc* (Figure 3E; Table S5). Frailty includes decline in muscle strength and coordination[47]; also, in support of the increased frailty of aged CD300f$^{-/-}$ mice, two different cohorts of female mice displayed motor coordination deficits at age 24 months (Figure 3L).

Cognitive decline, and in particular learning and memory, is another defining feature of aging.[48] To uncover putative differences in cognitive decline, CD300f$^{-/-}$ mice were exposed to two different tests for evaluating learning and memory: the novel object recognition (NOR) test that provides an index of recognition memory, and the Barnes maze test that evaluates spatial learning and memory. No differences were observed in the performance of 18-month-old females in the NOR test (Figure 4A). However, 24-month-old CD300f$^{-/-}$ females, but not 22-month-old males, displayed a decreased capacity for the recognition of a new object (Figures 4B, 4C, and S5E). In a similar fashion, while 12-month-old mice of both sexes did not show learning and memory alterations in the Barnes maze (Figures 4D, 4G, S5A, and S5C), 18-month-old CD300f$^{-/-}$ female and male mice began to show alterations in memory for the escape position (Figures 4E, 4H, S5B, and 5D). This loss of memory was also observed in CD300f$^{-/-}$ females at age 24 months (Figures 4F and 4I–4J).

Taken together, and in accordance with the putative increased aging phenotype of the CD300f$^{-/-}$ mice, our results show an age-dependent brain inflammaging, senescence, enhanced age and neurodegeneration of microglial/macrophage (DAM/DIM) state, frailty/motor coordination deficits, and cognitive decline.

Absence of CD300f induces age-related decrease in CNS glucose uptake

Early brain hypometabolism observed by ^{18}F-fluorodeoxyglucose positron emission tomography (^{18}F-FDG PET) scans is a hallmark of aging and is associated to AD and cognitive decline.[49] Alterations in brain microglial immune receptors such as TREM2 or GRN induce profound changes in microglial phenotype and brain function. Independently of the inflammatory profile of these TREM2$^{-/-}$ and GRN$^{-/-}$ brains, they share decreased global glucose uptake,[50,51] which, at least in the case of TREM2, is age dependent.[52] We reproduced these experiments using ^{18}F-FDG PET/computed tomography scans imaging in adult and aged (18 months old) CD300f$^{-/-}$ and WT mice. Although no changes were observed in adult mice, 18-month-old CD300f$^{-/-}$ female mice showed a decreased global brain ^{18}F-FDG uptake (Figures 5A–5C), an effect that was evident in all of the brain areas analyzed (Figure 5D). Of note, we only observed this effect in aged female but not aged male mice (Figure 5C). Remarkably, the studies describing reduction of glucose uptake in TREM2$^{-/-}$, TREM2^{T66M} AD mutation, or Grn$^{-/-}$ mice were performed only in females aged 8–12 months, and no data are available for male mice.[50–52]

Elevated blood lactate can decrease brain ^{18}FDG uptake due to a switch in energy substrate usage[53]; however, no alterations in blood lactate levels were observed in CD300f$^{-/-}$ mice under basal conditions (Figure 5E). Moreover, the decrease in brain glucose uptake was not due to alterations in circulating glucose availability as glycemia did not change under physiological conditions (Figure 1I). Taken together, these results suggest that microglia/macrophage CD300f may be involved in age-dependent brain glucose uptake reduction that contributes to cognitive decline. Whether the reduced glucose uptake represents neuronal death, reduced brain metabolism, or alternative substrate utilization of, for instance, lactate or ketone bodies needs to be determined.

Absence of CD300f induces macrophage metabolic alterations

Aging induces a decrease of glycolysis and oxidative phosphorylation rates in aged human and mice macrophages.[26] This prostaglandin E2-dependent decrease of metabolic fitness of microglia/macrophages was shown to worsen age-dependent cognitive decline.[26] Moreover, CD300f deficiency decreased microglial glycolysis and oxidative phosphorylation under inflammatory conditions in female mice.[7] However, it is not known whether this is restricted to microglial cells or if it extends to other monocyte/macrophage populations of the organism. Thus, we isolated WT and CD300f$^{-/-}$ BMDM and analyzed their metabolic profile using a Seahorse Extracellular Flux Analyzer. BMDM were cultured in limiting M-CSF (5 ng/mL) concentrations as this was shown to better uncover metabolic fitness alterations.[27] Female CD300f$^{-/-}$ BMDM showed reduced basal extracellular acidification rates (ECAR) (Figure 6A) and basal mitochondrial oxygen

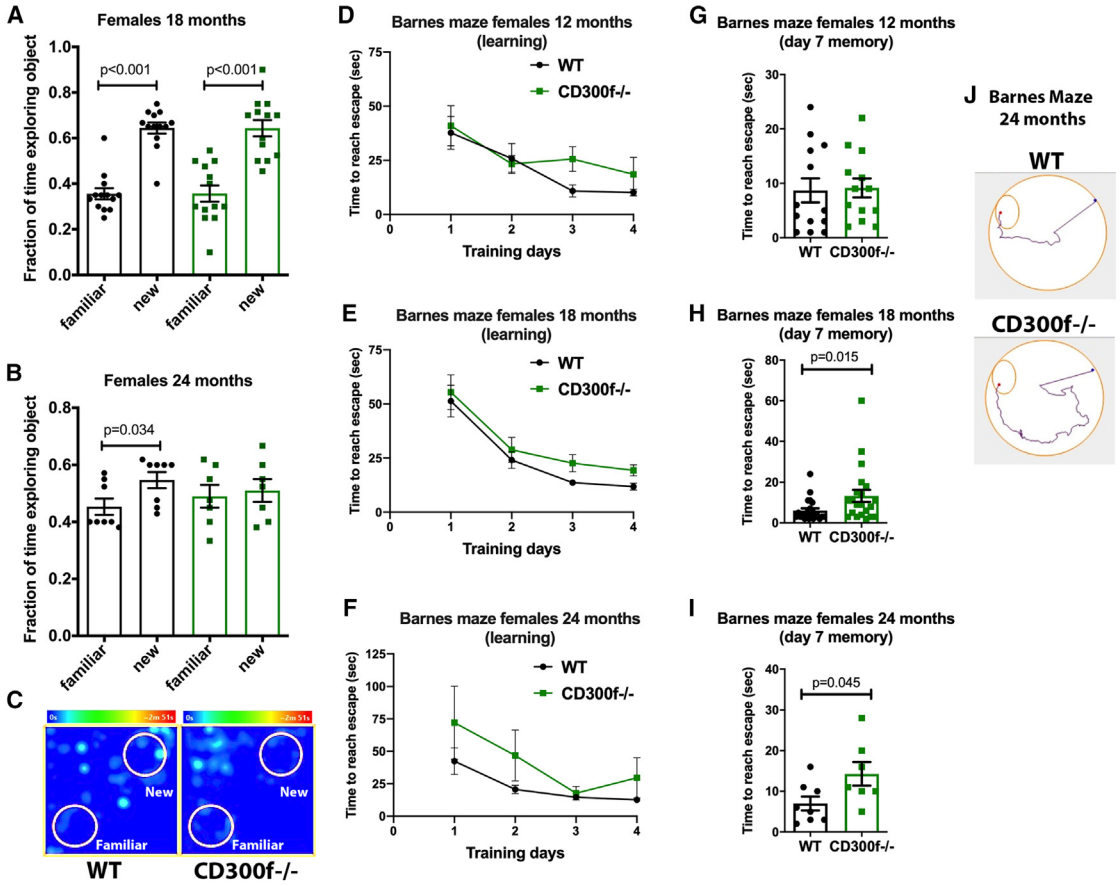

Figure 4. Absence of CD300f induces age-related cognitive decline

WT and CD300f$^{-/-}$ mice were followed for 24 months using the novel object recognition (NOR) and Barnes maze tests. CD300$^{-/-}$ females at 18 months showed no alterations in the NOR test (A), but lost the ability to recognize a new object at age 24 months (B and C). In the Barnes maze test experiments, CD300f$^{-/-}$ females did not show significant alterations in the time needed to learn which was the escape hole at age 12, 18, and 24 months (D, E, and F, respectively), or in memory 3 days after the last learning session at age 12 months (G) (day 7 from the beginning of the test). However, CD300f$^{-/-}$ females showed increased time for reaching the escape hole at age 18 and 24 months (H, I, and J).

consumption rates (OCR) (Figure 6B). Moreover, they also showed a decrease in maximum respiration rates and spare respiratory capacity, indicative of an impaired capacity for metabolic reprograming in response to a sudden increase in energy demands (Figures 6C and 6D). No significant differences were observed in the ATP-dependent and ATP-independent OCR of WT and CD300f$^{-/-}$ BMDM (Figure S6). However, male CD300f$^{-/-}$ macrophages did not show alterations in basal OCR (Figures 6E and 6G) nor in basal ECAR (Figures 6F and 6H), and only a tendency to decreased spared respiratory capacity. Moreover, inhibition of mitochondrial respiration induced the expected increase in ECAR in WT and CD300f$^{-/-}$ male BMDM (Figure 6F), while female CD300f$^{-/-}$ BMDM were not able to reprogram their metabolism under these conditions (Figure 6F). The absence of CD300f also demonstrated an alteration at the level of mechanistic target of rapamycin (mTOR) activation, a central coordinator of cellular metabolism in female BMDM. No changes were observed in the phosphorylation of the mTOR targets S6 or 4EBP1 under basal culture conditions with high MCSF concentrations (20 ng/mL), in MCSF limiting conditions (5 ng/mL), or after inhibition of mTOR by rapamycin (Figures 6I and 6J). However, after LPS treatment, WT BMDM increased mTOR activity, as observed by the increase in the phosphorylation of its target S6, while CD300f$^{-/-}$ BMDM did not (Figures 6I and 6J). Also, phosphorylated 4EBP1 showed a trend toward a decrease in CD300f$^{-/-}$ LPS-treated BMDM. Taken together, these data suggest that the absence of CD300f derails macrophage metabolic fitness with a more pronounced effect in females. In addition to this effect in microglial cells,[7] it could contribute to the diverse age-associated effects observed in CD300f$^{-/-}$ mice such as increased cognitive decline.

DISCUSSION

The main finding of this study is that CD300f$^{-/-}$ male and female mice have shortened lifespan and healthspan. The underlying causes of death are probably multifactorial and variable depending on the subject, as would be expected for aging. CD300f deficiency leads to widespread deficits in microglia/macrophage

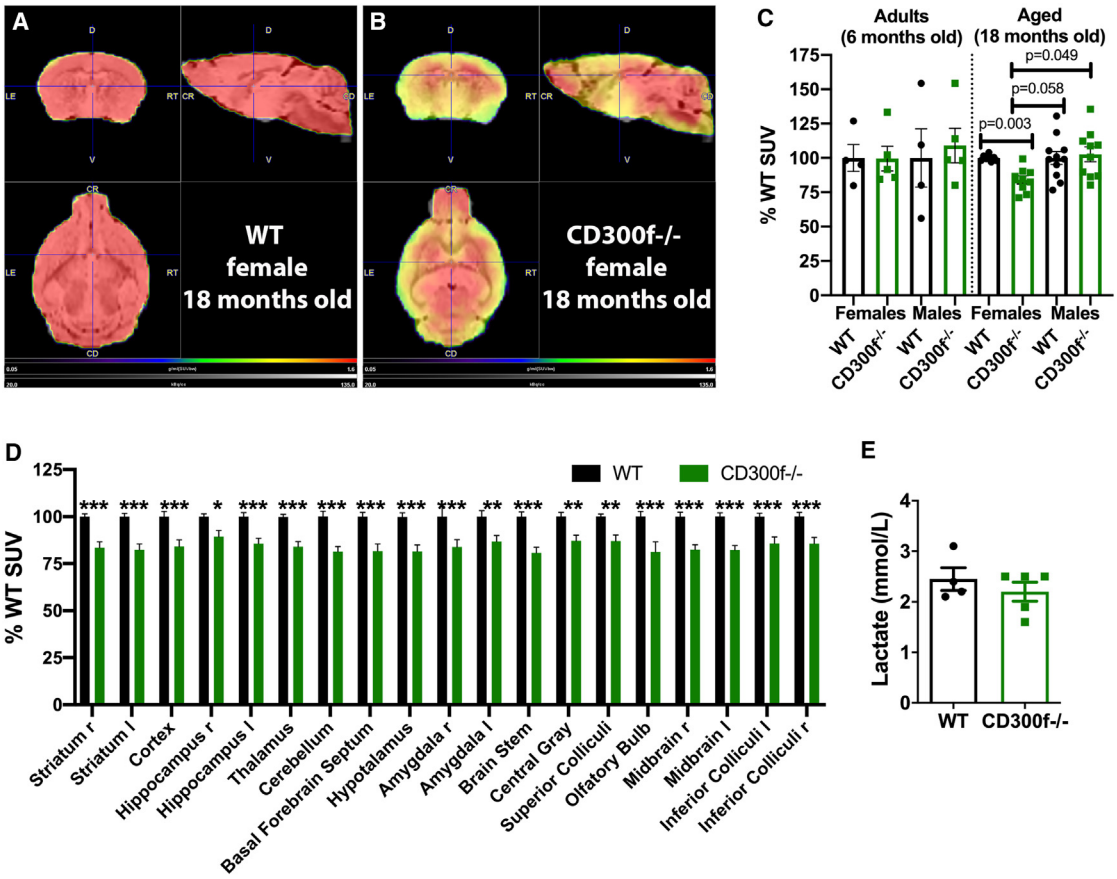

Figure 5. Absence of CD300f reduces brain glucose uptake in aged females

Adult (6 months) and aged (18 months) WT and CD300f$^{-/-}$ male and female mice were subjected to ^{18}F-FDG PET/computed tomography scans (A and B). Aged CD300f$^{-/-}$ female mice showed a reduced ^{18}F-FDG standard uptake value (SUV) when compared with the other groups (C) (n = 8 for WT and n = 9 for CD300f$^{-/-}$ 18-month-old female mice, Brown-Forsythe ANOVA test followed by Dunnett's T3 multiple comparisons test). This reduction was observed in all brain areas analyzed (D) (r, right; l, left; *p < 0.05, **p < 0.01, ***p < 0.001 by two-tailed Student's t test). The standardized uptake value (SUV) units are the average activity per volume unit (kBq/cc) subsequently corrected for injected radioactivity and mouse weight. No alterations were observed in basal blood lactate levels (E) (18-month-old female mice).

metabolic fitness, which, with aging, may alter the function of macrophages of different tissues, inducing inflammaging, senescence, cognitive decline, proteostasis alteration, systemic metabolic changes, and frailty.

Maximum lifespan has been the foremost criteria in aging research. However, while informative, longevity by itself is an incomplete estimation of health, assessment of physiologic, behavioral, and pathological states of the mice coupled to lifespan extension generates a more accurate characterization of the aging process and its associated diseases.[54] Defining what constitutes health and therefore healthy aging in mice or humans is not a simple task. Some evidence points toward the notion that CD300f$^{-/-}$ mice display several hallmarks of aging and aging-associated pathologies that are associated to decreased healthspan. They include earlier emergence of different neoplasms, chronic low-grade organismal inflammation or inflammaging, frailty, alterations in brain proteostasis pathways, increased brain senescence and cognitive decline, and, in the case of females, also systemic metabolic alterations.

An important process that makes it difficult to understand the possible cause of death during aging is the fact that biological age differs from chronological age and between subjects.[55] We were unable to determine one specific pathology associated to CD300f deficiency, as would be anticipated for the non-synchronous aging process in combination with the wide variety of pathologies associated with aging. In fact, an important dispersion of the data was observed with time, supporting differences in chronological and biological age and the gradual but unsynchronous emergence of aging-associated pathologies. Although we have not ruled out every possible cause of death, we have analyzed many relevant biological parameters. No general alterations were observed, neither in clinical blood markers of renal and hepatic pathologies nor in most blood cell counts until age 18 months. Scattered CD300f$^{-/-}$ mice showed pathological alterations in different systems as strongly reduced platelet counts (thrombocytopenia), increased spleen weight (putatively indicative of autoimmune diseases), hypoglycemia, or anemia. Thus, our data point to

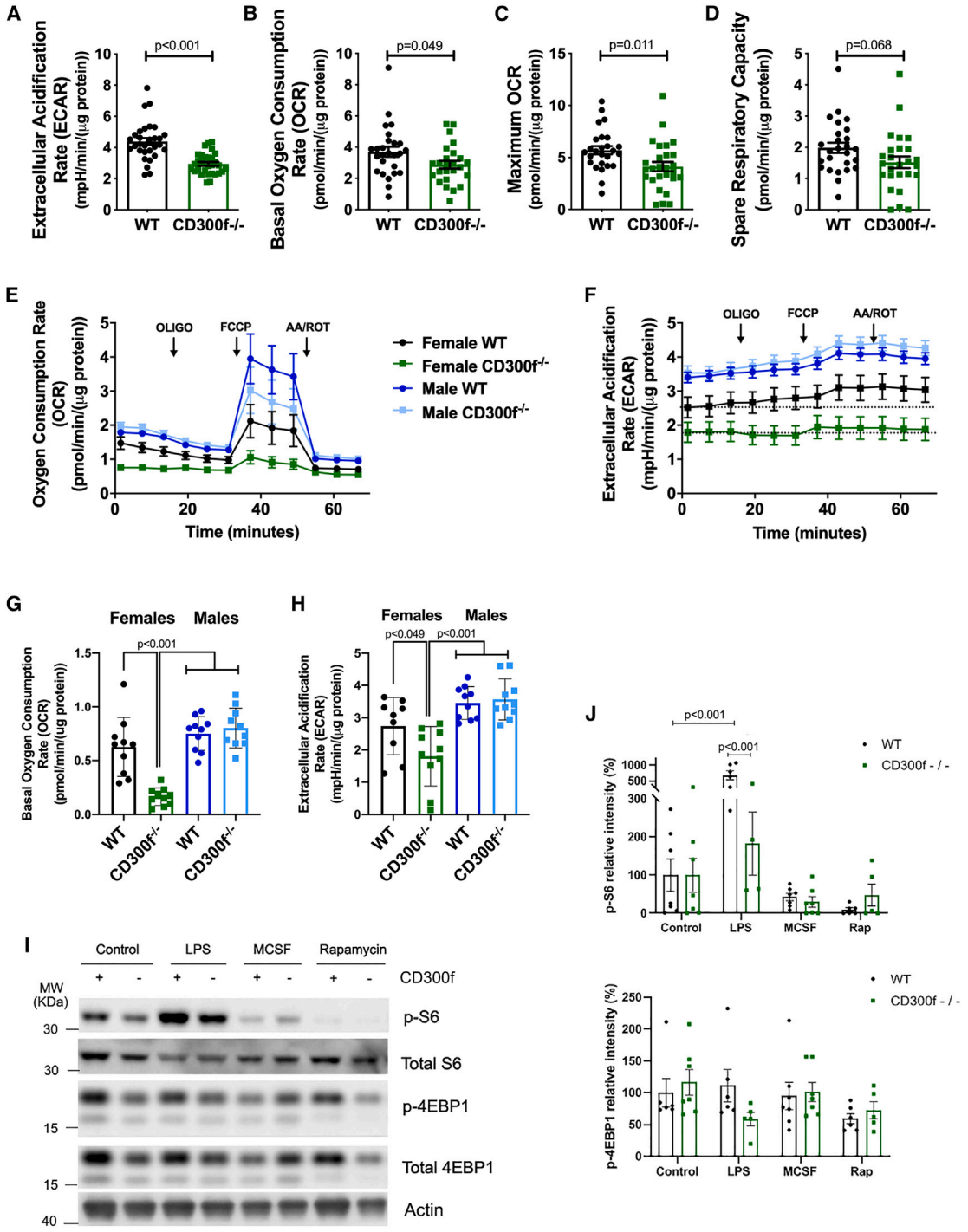

Figure 6. Absence of CD300f alters macrophage metabolism

Basal extracellular acidification rate (ECAR) (A) and oxygen consumption rate (OCR) (B) were decreased in CD300f$^{-/-}$ BMDM from adult female mice under limiting MCSF concentrations (5 ng/mL) when compared with WT. Moreover, they also showed impaired maximum respiration rates (C) and spare respiratory capacity (D). The OCR and ECAR under different conditions were compared between female and male BMDM cultures (E–H). Female BMDM cultures were incubated with 20 ng/mL MCSF, and treated with vehicle, 100 ng/mL LPS, or 100 µM rapamycin (Rap), or only incubated with 5 ng/mL MCSF, and the phosphorylation of several mTOR signaling pathway components was analyzed by western blot (I and J).

the absence of an important unique underlying pathology in CD300f$^{-/-}$ mice; however, they do point to the expected general causes of death related to aging. Accordingly, increased plasma GGT was observed in CD300f$^{-/-}$ female mice that had to be euthanized due to ethical endpoint considerations, and elevated circulating levels of this enzyme have been associated with all causes of mortality.[32]

We have found several sex-related alterations in aged CD300f$^{-/-}$ males and females, such as systemic metabolic alterations, macrophage metabolism, reduced brain glucose uptake, or earlier cognitive decline in females. For instance, hepatic gluconeogenesis capacity decreased with age in WT female mice, and this effect occurred earlier in CD300f$^{-/-}$ female mice than in WT mice, and was not observed in male mice. Also, CD300f$^{-/-}$ female mice showed reduced capacity for discriminating a new object in the NOR test at age 24 months, while CD300f$^{-/-}$ male mice did not. This correlates with the known epidemiology of AD dementia, which shows that females are more affected.[56] Accordingly, sex differences regarding the role of CD300f have also been described for psychiatric conditions such as depression and anxiety.[7,24] Better understanding of sex and gender differences is leading to improved care and treatment for both women and men, and identifying new mechanisms and molecular targets will provide better treatment and care for both. However, regarding lifespan, we observed that CD300f$^{-/-}$ mice of both sexes show a similar reduction. This could imply that the reduced lifespan in both females and males is related to the general aging processes not dependent on sex, or alternatively that both sexes display different causes of death due to different age-associated pathologies with similar reductions in lifespan. This should be analyzed in detail in further studies.

CD300f has been shown to regulate microglial phenotype, and here we extend these data to other macrophage populations. This could expand the effect of CD300f deficiency to the whole organism, affecting tissue-resident macrophages around the body and in different organs. As a putative DAMP receptor, CD300f may cooperate with other receptors such as TREM2 to sense DAMPs and other toxic lipids derived from chronic low-grade tissue damage during aging,[57] clearing them from the extracellular space and at the same time dampening the inflammatory reaction, contributing to the reestablishment of homeostasis. CD300f can in fact also inhibit the proinflammatory signaling of PAMP receptors such as Toll-like receptors.[58] This is particularly important for the CNS, as it tolerates inflammation badly; also, it contains an important amount of lipids and lipid debris generated by normal myelin turnover, after a lesion, or under chronic neurodegenerative conditions. According to a recent study,[41] DAM microglia are embryonically derived and would appear only in the context of neurodegeneration and not significantly during normal aging. Conversely, the same study suggested that monocyte-derived DIMs would accumulate mainly with age, neuroinflammation and, at least, AD-related neurodegeneration. Our analysis of microglial and macrophage phenotype by RNA-seq showed increased DAM and DIM stages in 30-month-old female CD300f$^{-/-}$ mice. Thus, these data would point toward increased aging but also neurodegenerative processes in the CD300f$^{-/-}$ brain. Moreover, in opposition to TREM2, CD300f would contribute to the maintenance of the microglial homeostatic phenotype during aging. If the maintenance of the microglial homeostatic phenotype is necessary for healthy brain aging or, on the contrary, if the DAM phenotype is an important reaction of microglial cells to cope with aging-associated brain changes needs to be established in future studies.

The aging-related longevity pathways of growth, metabolism, nutrient sensing, autophagy, and stress response are intertwined, as demonstrated by many connected effector proteins that interact either directly or through their network neighbors. Strategies such as dampening mTOR or activating AMP-activated protein kinase modulate aging and extend lifespan.[59] These connected signaling pathways indicate the interplay between metabolism and molecular and cellular defenses against aging and its associated pathologies such as AD. A robust example is that aged macrophages display metabolic alterations and induce cognitive decline, an effect that is reversed by the restitution of macrophage metabolism.[26] There is transcriptomic and biochemical experimental evidence for the *in vivo* importance of CD300f−/− in microglial metabolic fitness,[7] and CD300f has also been recently shown to be among the top 20 upregulated genes in microglia of naive mice after specific genetic microglial mTOR activation.[60] The same work reported that activation of microglial mTOR induced increased microglia homing to Aβ plaques, reduced accumulation of plaques, maintained spine density, and improved memory in 5xFAD mice. We show here that, as occurs with microglia,[7] the absence of CD300f in macrophages alters their metabolic fitness, affecting mitochondrial function and mTOR activation. In this context, our data suggest that, because of its role in metabolic activation and autophagy, CD300f may function as a costimulatory molecule that sustains microglia/macrophage transition to different relevant phenotypes that are triggered by various receptors engaged by tissue injury or dysfunction, such as apoptotic cells, debris, Aβ plaques, and myelin damage. In this way, CD300f malfunction would affect myelin debris phagocytosis/myelin recycling, lipoprotein interaction and lipid metabolism, neuroinflammation, and synaptic pruning, ultimately enhancing neurodegeneration and cognitive decline. Understanding CD300f function in the CNS, the role of single-nucleotide polymorphisms or their therapeutic CD300f activation could contribute to the design of new treatment paradigms for AD and other aged-related neuropathologies.

In wider terms, this work suggests that the study of the biology of immune receptors in the context of aging could contribute to the elucidation of novel predictors of both health and lifespan, and may identify therapeutic targets for attenuating aging and abrogating age-related diseases. More than 90% of individuals over 65 years of age have at least one chronic disease, such as cardiovascular disease, cancer, dementia, diabetes, osteoarthritis, or osteoporosis, and >70% have at least two such conditions.[61] Thus, on a wider perspective, therapeutic strategies to target fundamental aging mechanisms, as opposed to treating each age-associated disease separately, could have a tremendous effect on global health.

Limitations of the study

Although we have employed multiple approaches and thoroughly analyzed many parameters to discover a single specific cause of death of CD300f$^{-/-}$ mice, we could not determine a single alteration leading to the reduced lifespan. We could not follow some parameters such as cardiovascular alterations. However, aging also induces cardiovascular alterations and thus this could fit in the hypothesis of CD300f participating in maintaining health during aging. Another limitation was determined by the cost of these experiments and the necessity to obtain animals for analysis of the putative causes of death and mechanisms of injury or aging. We decided to stop the experiments before losing all CD300f$^{-/-}$ mice (despite close follow-up many times the animals were found dead and could not be collected) and thus did not obtain data regarding the median lifespan of the WT mice. Total male data show a 104-week median survival for CD300f$^{-/-}$ mice and at least 136 weeks for WT male mice (Figure S1D). Total female median survival was 121 weeks for CD300f$^{-/-}$ mice and at least 134 weeks for WT mice (Figure S1C), indicating a decrease of around 23% for males and 10% for females. However, although this estimation is probably similar to the real median survival for male mice (data from ≅55% mice alive), it is an underestimation for female mice (data from ≅65% mice alive) as the data used for median survival for WT mice are the latest data available at the end of the experiment. In this context, when analyzing the putative progression of survival curves, the estimated reduction in lifespan for female mice is probably similar to that of male mice. We are aware that the data presented here may not be true for human aging. Data relating CD300f with longevity, for instance, in centenarian human cohorts would strengthen the hypothesis proposed in this work. Another limitation of this study is that this manuscript analyzed bulk RNA-seq data obtained from whole brains of aged mice, and the data represent an average of genes expressed by different cell types and in different brain regions. GSEA analysis clearly showed interesting changes in microglia/macrophage phenotypes, although more specific experiments (e.g., RNA-seq of FACS-sorted microglia or single-cell RNA-seq) are required to discard effects of the change of cell proportions with aging or genotype, and further dissect their phenotypes. Finally, because CD300f is expressed on circulating monocytes, tissue-resident macrophages in the periphery and other myeloid cells, it will be important to unravel the relative role of CD300f expression in peripheral cells versus CD300f expressed by microglia and BAMs in the nervous system. Addressing these questions will contribute to a more comprehensive understanding of the significance of CD300f in the context of neurodegeneration and aging.

STAR★METHODS

Detailed methods are provided in the online version of this paper and include the following:

- KEY RESOURCES TABLE
- RESOURCE AVAILABILITY
  - Lead contact
  - Materials availability
  - Data and code availability
- EXPERIMENTAL MODEL AND STUDY PARTICIPANT DETAILS
- METHOD DETAILS
  - Complete blood count
  - Hepatic and renal function
  - Metabolic tests: Glucose tolerance test, pyruvate tolerance test, and insulin tolerance test
  - Histological and immunohistochemistry procedures
  - RNA extraction and qPCR
  - RNA sequencing and transcriptomic analysis
  - Flow cytometry
  - Novel object recognition (NOR)
  - Barnes Maze test
  - Parallel rod floor test (ataxia)
  - Bone marrow derived macrophages cultures
  - Measurement of oxygen consumption rates
  - Western blotting
  - PET/CT imaging
- QUANTIFICATION AND STATISTICAL ANALYSIS

SUPPLEMENTAL INFORMATION

Supplemental information can be found online at https://doi.org/10.1016/j.celrep.2023.113269.

ACKNOWLEDGMENTS

This work has been supported by grants from Comisión Sectorial de Investigación Científica (CSIC-UDELAR I+D 2020 ID 184 and ID 424, Espacio Interdisciplinario - UDELAR Centros 2015 and Espacio Interdisciplinario-UDELAR Grupos 2021), Uruguay; PEDECIBA, Uruguay; FOCEM (MERCOSUR Structural Convergence Fund), COF 03/1111; Banco de Seguros del Estado (BSE), Uruguay; Ministerio de Ciencia e Innovación, Gobierno de España (PID2021-123272OB-I0/Financiado por MCIN/AEI/10.13039/501100011033/ y por FEDER Una manera de hacer Europa), and International Centre for Genetic Engineering and Biotechnology (ICGEB, CRP/URY19-01). N.L. is a recipient of a Marie Skłodowska-Curie Individual Fellowship (H2020-MSCA-IF-2020 no. 101030280). We thank Mauro Costa-Mattioli for interesting discussions; and Florencia Fontes and Mariela Santos and the rest of the URBE Facultad de Medicina UDELAR personnel, and Sergio Ancheta and the rest of the UBAL-Institut Pasteur de Montevideo personnel.

AUTHOR CONTRIBUTIONS

H.P., M.L.N.-D., F.E., and N.L. conceived the study. F.E. performed most of the experiments. B.P., F.A.C., N.L., M.L.N.-D., P.S.-M., A.C.-G., A.P., L.R., J.R.-D., V.P.-T., and M.B. performed the experiments. N.R. performed all bioinformatics analysis. L.R., A.P., H.P., and E.S. performed and analyzed PET experiments. M.N.M., G.S., A.P.M., and M.C. generated the CD300f$^{-/-IPMon}$ mice. F.E., H.P., N.R., C.E., C.Q., C.M., and N.L. analyzed and discussed the results. H.P. drafted the original manuscript and F.E., N.R., C.E., M.C., N.L., E.S., C.M., P.S.-M., and C.Q. contributed to the edition of the final version. All authors have read and agreed to the published version of the manuscript.

DECLARATION OF INTERESTS

The authors declare no competing interests.

Received: March 10, 2023
Revised: August 25, 2023
Accepted: September 28, 2023
Published: October 20, 2023

REFERENCES

1. Jaitin, D.A., Adlung, L., Thaiss, C.A., Weiner, A., Li, B., Descamps, H., Lundgren, P., Bleriot, C., Liu, Z., Deczkowska, A., et al. (2019). Lipid-Associated Macrophages Control Metabolic Homeostasis in a Trem2-Dependent Manner. Cell *178*, 686–698.e14. https://doi.org/10.1016/j.cell.2019.05.054.
2. Wynn, T.A., and Vannella, K.M. (2016). Macrophages in Tissue Repair, Regeneration, and Fibrosis. Immunity *44*, 450–462. https://doi.org/10.1016/j.immuni.2016.02.015.
3. Schwarz, F., Pearce, O.M.T., Wang, X., Samraj, A.N., Läubli, H., Garcia, J.O., Lin, H., Fu, X., Garcia-Bingman, A., Secrest, P., et al. (2015). Siglec receptors impact mammalian lifespan by modulating oxidative stress. Elife *4*, e06184. https://doi.org/10.7554/eLife.06184.
4. Podleśny-Drabiniok, A., Marcora, E., and Goate, A.M. (2020). Microglial Phagocytosis: A Disease-Associated Process Emerging from Alzheimer's Disease Genetics. Trends Neurosci. *43*, 965–979. https://doi.org/10.1016/j.tins.2020.10.002.
5. Lewcock, J.W., Schlepckow, K., Di Paolo, G., Tahirovic, S., Monroe, K.M., and Haass, C. (2020). Emerging Microglia Biology Defines Novel Therapeutic Approaches for Alzheimer's Disease. Neuron *108*, 801–821. https://doi.org/10.1016/j.neuron.2020.09.029.
6. Perugorria, M.J., Esparza-Baquer, A., Oakley, F., Labiano, I., Korosec, A., Jais, A., Mann, J., Tiniakos, D., Santos-Laso, A., Arbelaiz, A., et al. (2019). Non-parenchymal TREM-2 protects the liver from immune-mediated hepatocellular damage. Gut *68*, 533–546. https://doi.org/10.1136/gutjnl-2017-314107.
7. Lago, N., Kaufmann, F.N., Negro-Demontel, M.L., Alí-Ruiz, D., Ghisleni, G., Rego, N., Arcas-García, A., Vitureira, N., Jansen, K., Souza, L.M., et al. (2020). CD300f immunoreceptor is associated with major depressive disorder and decreased microglial metabolic fitness. Proc. Natl. Acad. Sci. USA *117*, 6651–6662. https://doi.org/10.1073/pnas.1911816117.
8. Tian, L., Choi, S.C., Lee, H.N., Murakami, Y., Qi, C.F., Sengottuvelu, M., Voss, O., Krzewski, K., and Coligan, J.E. (2016). Enhanced efferocytosis by dendritic cells underlies memory T-cell expansion and susceptibility to autoimmune disease in CD300f-deficient mice. Cell Death Differ. *23*, 1086–1096. https://doi.org/10.1038/cdd.2015.161.
9. Deczkowska, A., Keren-Shaul, H., Weiner, A., Colonna, M., Schwartz, M., and Amit, I. (2018). Disease-Associated Microglia: A Universal Immune Sensor of Neurodegeneration. Cell *173*, 1073–1081. https://doi.org/10.1016/j.cell.2018.05.003.
10. Alvarez-Errico, D., Aguilar, H., Kitzig, F., Brckalo, T., Sayós, J., and López-Botet, M. (2004). IREM-1 is a novel inhibitory receptor expressed by myeloid cells. Eur. J. Immunol. *34*, 3690–3701.
11. Alvarez-Errico, D., Sayós, J., and López-Botet, M. (2007). The IREM-1 (CD300f) inhibitory receptor associates with the p85alpha subunit of phosphoinositide 3-kinase. J. Immunol. *178*, 808–816.
12. Martínez-Barriocanal, A., Comas-Casellas, E., Schwartz, S., Jr., Martín, M., and Sayós, J. (2010). CD300 heterocomplexes, a new and family-restricted mechanism for myeloid cell signaling regulation. J. Biol. Chem. *285*, 41781–41794. https://doi.org/10.1074/jbc.M110.140889.
13. Xi, H., Katschke, K.J., Jr., Helmy, K.Y., Wark, P.A., Kljavin, N., Clark, H., Eastham-Anderson, J., Shek, T., Roose-Girma, M., Ghilardi, N., and van Lookeren Campagne, M. (2010). Negative regulation of autoimmune demyelination by the inhibitory receptor CLM-1. J. Exp. Med. *207*, 7–16, jem.20091508 [pii]. https://doi.org/10.1084/jem.20091508.
14. Tian, L., Choi, S.C., Murakami, Y., Allen, J., Morse, H.C., Qi, C.F., Krzewski, K., and Coligan, J.E. (2014). P85alpha recruitment by the CD300f phosphatidylserine receptor mediates apoptotic cell clearance required for autoimmunity suppression. Nat. Commun. *5*, 3146. https://doi.org/10.1038/ncomms4146.
15. Izawa, K., Yamanishi, Y., Maehara, A., Takahashi, M., Isobe, M., Ito, S., Kaitani, A., Matsukawa, T., Matsuoka, T., Nakahara, F., et al. (2012). The receptor LMIR3 negatively regulates mast cell activation and allergic responses by binding to extracellular ceramide. Immunity *37*, 827–839. https://doi.org/10.1016/j.immuni.2012.08.018.
16. Peluffo, H., Alí-Ruiz, D., Ejarque-Ortíz, A., Heras-Alvarez, V., Comas-Casellas, E., Martínez-Barriocanal, A., Kamaid, A., Alvarez-Errico, D., Negro, M.L., Lago, N., et al. (2012). Overexpression of the immunoreceptor CD300F has a neuroprotective role in a model of acute brain injury. Brain Pathol. *22*, 318–328. https://doi.org/10.1111/j.1750-3639.2011.00537.x.
17. Ejarque-Ortiz, A., Solà, C., Martínez-Barriocanal, Á., Schwartz, S., Martín, M., Peluffo, H., and Sayós, J. (2015). The receptor CMRF35-like molecule-1 (CLM-1) enhances the production of LPS-induced pro-inflammatory mediators during microglial activation. PLoS One *10*, e0123928. https://doi.org/10.1371/journal.pone.0123928.
18. Bennett, M.L., Bennett, F.C., Liddelow, S.A., Ajami, B., Zamanian, J.L., Fernhoff, N.B., Mulinyawe, S.B., Bohlen, C.J., Adil, A., Tucker, A., et al. (2016). New tools for studying microglia in the mouse and human CNS. Proc. Natl. Acad. Sci. USA *113*, E1738–E1746. https://doi.org/10.1073/pnas.1525528113.
19. Torres-Espín, A., Hernández, J., and Navarro, X. (2013). Gene expression changes in the injured spinal cord following transplantation of mesenchymal stem cells or olfactory ensheathing cells. PLoS One *8*, e76141. https://doi.org/10.1371/journal.pone.0076141.
20. Lloyd, A.F., Davies, C.L., Holloway, R.K., Labrak, Y., Ireland, G., Carradori, D., Dillenburg, A., Borger, E., Soong, D., Richardson, J.C., et al. (2019). Central nervous system regeneration is driven by microglia necroptosis and repopulation. Nat. Neurosci. *22*, 1046–1052.
21. Ising, C., Venegas, C., Zhang, S., Scheiblich, H., Schmidt, S.V., Vieira-Saecker, A., Schwartz, S., Albasset, S., McManus, R.M., Tejera, D., et al. (2019). NLRP3 inflammasome activation drives tau pathology. Nature *575*, 669–673. https://doi.org/10.1038/s41586-019-1769-z.
22. Danik, J.S., Paré, G., Chasman, D.I., Zee, R.Y.L., Kwiatkowski, D.J., Parker, A., Miletich, J.P., and Ridker, P.M. (2009). Novel loci, including those related to Crohn disease, psoriasis, and inflammation, identified in a genome-wide association study of fibrinogen in 17 686 women: the Women's Genome Health Study. Circ. Cardiovasc. Genet. *2*, 134–141. https://doi.org/10.1161/CIRCGENETICS.108.825273.
23. Ban, M., McCauley, J.L., Zuvich, R., Baker, A., Bergamaschi, L., Cox, M., Kemppinen, A., D'Alfonso, S., Guerini, F.R., Lechner-Scott, J., et al. (2010). A non-synonymous SNP within membrane metalloendopeptidase-like 1 (MMEL1) is associated with multiple sclerosis. Gene Immun. *11*, 660–664. https://doi.org/10.1038/gene.2010.36.
24. Kaufmann, F.N., Lago, N., Alí-Ruiz, D., Jansen, K., Souza, L.D.M., Silva, R.A., Lara, D.R., Ghisleni, G., Peluffo, H., and Kaster, M.P. (2021). Sex-dependent role of CD300f immune receptor in generalized anxiety disorder. Brain Behav. Immun. Health *11*, 100191. https://doi.org/10.1016/j.bbih.2020.100191.
25. Grabert, K., Michoel, T., Karavolos, M.H., Clohisey, S., Baillie, J.K., Stevens, M.P., Freeman, T.C., Summers, K.M., and McColl, B.W. (2016). Microglial brain region-dependent diversity and selective regional sensitivities to aging. Nat. Neurosci. *19*, 504–516. https://doi.org/10.1038/nn.4222.
26. Minhas, P.S., Latif-Hernandez, A., McReynolds, M.R., Durairaj, A.S., Wang, Q., Rubin, A., Joshi, A.U., He, J.Q., Gauba, E., Liu, L., et al. (2021). Restoring metabolism of myeloid cells reverses cognitive decline in ageing. Nature *590*, 122–128. https://doi.org/10.1038/s41586-020-03160-0.
27. Beatty, W.L., Loboda, A.A., Huang, S.C.C., Ulrich, J.D., Sergushichev, A., Ulland, T.K., Song, W.M., Zhou, Y., Cairns, N.J., Kambal, A., et al. (2017). TREM2 Maintains Microglial Metabolic Fitness in Alzheimer ' s Disease Article TREM2 Maintains Microglial Metabolic Fitness in Alzheimer ' s Disease. Cell *170*, 649–663.e13. https://doi.org/10.1016/j.cell.2017.07.023.
28. Alexi, N., Inge, R.H., Nicole, G.C., Johannes, C.M.S., Miao, Y., Rong, H., Claudia, Z.H., Monique, P., Jiayang, X., Yin, W., et al. (2019). Brain cell

type – specific enhancer – promoter interactome maps and disease-risk association. Science *1139*, 1134–1139.

29. Novikova, G., Kapoor, M., Tcw, J., Abud, E.M., Efthymiou, A.G., Chen, S.X., Cheng, H., Fullard, J.F., Bendl, J., Liu, Y., et al. (2021). Integration of Alzheimer's disease genetics and myeloid genomics identifies disease risk regulatory elements and genes. Nat. Commun. *12*, 1610. https://doi.org/10.1038/s41467-021-21823-y.
30. Hamilton, S.E., Badovinac, V.P., Beura, L.K., Pierson, M., Jameson, S.C., Masopust, D., and Griffith, T.S. (2020). New Insights into the Immune System Using Dirty Mice. J. Immunol. *205*, 3–11. https://doi.org/10.4049/jimmunol.2000171.
31. Pettan-Brewer, C., and M Treuting, P. (2011). Practical pathology of aging mice. Pathobiol. Aging & Age-related Dis. *1*, 7202. https://doi.org/10.3402/pba.v1i0.7202.
32. Ndrepepa, G., Colleran, R., and Kastrati, A. (2018). Gamma-glutamyl transferase and the risk of atherosclerosis and coronary heart disease. Clin. Chim. Acta *476*, 130–138. https://doi.org/10.1016/j.cca.2017.11.026.
33. Franceschi, C., Garagnani, P., Parini, P., Giuliani, C., and Santoro, A. (2018). Inflammaging: a new immune–metabolic viewpoint for age-related diseases. Nat. Rev. Endocrinol. *14*, 576–590. https://doi.org/10.1038/s41574-018-0059-4.
34. Rozenberg, P., Reichman, H., Zab-Bar, I., Itan, M., Pasmanik-Chor, M., Bouffi, C., Qimron, U., Bachelet, I., Fulkerson, P.C., Rothenberg, M.E., and Munitz, A. (2017). CD300f: IL-5 cross-talk inhibits adipose tissue eosinophil homing and subsequent IL-4 production. Sci. Rep. *7*, 5922. https://doi.org/10.1038/s41598-017-06397-4.
35. Morgantini, C., Jager, J., Li, X., Levi, L., Azzimato, V., Sulen, A., Barreby, E., Xu, C., Tencerova, M., Näslund, E., et al. (2019). Liver macrophages regulate systemic metabolism through non-inflammatory factors. Nat. Metab. *1*, 445–459. https://doi.org/10.1038/s42255-019-0044-9.
36. Hickman, S.E., Kingery, N.D., Ohsumi, T.K., Borowsky, M.L., Wang, L.c., Means, T.K., and El Khoury, J. (2013). The microglial sensome revealed by direct RNA sequencing. Nat. Neurosci. *16*, 1896–1905. https://doi.org/10.1038/nn.3554.
37. Ravichandran, M., Priebe, S., Grigolon, G., Rozanov, L., Groth, M., Laube, B., Guthke, R., Platzer, M., Zarse, K., and Ristow, M. (2018). Impairing L-Threonine Catabolism Promotes Healthspan through Methylglyoxal-Mediated Proteohormesis. Cell Metabol. *27*, 914–925.e5. https://doi.org/10.1016/j.cmet.2018.02.004.
38. Saul, D., Kosinsky, R.L., Atkinson, E.J., Doolittle, M.L., Zhang, X., LeBrasseur, N.K., Pignolo, R.J., Robbins, P.D., Niedernhofer, L.J., Ikeno, Y., et al. (2022). A new gene set identifies senescent cells and predicts senescence-associated pathways across tissues. Nat. Commun. *13*, 4827. https://doi.org/10.1038/s41467-022-32552-1.
39. David, E., Baruch, K., Lara-Astaiso, D., Matcovitch-Natan, O., Dvir-Sztern-feld, R., Ulland, T.K., Keren-shaul, H., Spinrad, A., Weiner, A., Toth, B., et al. (2017). Article A Unique Microglia Type Associated with Restricting Development of Alzheimer ' s Disease Article A Unique Microglia Type Associated with Restricting Development of Alzheimer ' s Disease. Cell *169*, 1276–1290.e17. https://doi.org/10.1016/j.cell.2017.05.018.
40. El Fatimy, R., Beckers, L., O'Loughlin, E., Baufeld, C., Calcagno, N., Krasemann, S., Madore, C., Cialic, R., Xu, Y., Fanek, Z., et al. (2017). The TREM2-APOE Pathway Drives the Transcriptional Phenotype of Dysfunctional Microglia in Neurodegenerative Diseases Article The TREM2-APOE Pathway Drives the Transcriptional Phenotype of Dysfunctional Microglia in Neurodegenerative Diseases. Immunity *47*, 566–581.e9. https://doi.org/10.1016/j.immuni.2017.08.008.
41. Silvin, A., Uderhardt, S., Piot, C., Da Mesquita, S., Yang, K., Geirsdottir, L., Mulder, K., Eyal, D., Liu, Z., Bridlance, C., et al. (2022). Dual ontogeny of disease-associated microglia and disease inflammatory macrophages in aging and neurodegeneration. Immunity *55*, 1448–1465.e6. https://doi.org/10.1016/j.immuni.2022.07.004.
42. Marschallinger, J., Iram, T., Zardeneta, M., Lee, S.E., Lehallier, B., Haney, M.S., Pluvinage, J.V., Mathur, V., Hahn, O., Morgens, D.W., et al. (2020). Lipid-droplet-accumulating microglia represent a dysfunctional and proinflammatory state in the aging brain. Nat. Neurosci. *23*, 194–208. https://doi.org/10.1038/s41593-019-0566-1.
43. Li, W., Li, X., and Miller, R.A. (2014). ATF4 activity: A common feature shared by many kinds of slow-aging mice. Aging Cell *13*, 1012–1018. https://doi.org/10.1111/acel.12264.
44. Mitnitski, A.B., Mogilner, A.J., and Rockwood, K. (2001). Accumulation of deficits as a proxy measure of aging. Sci. World J. *1*, 323–336. https://doi.org/10.1100/tsw.2001.58.
45. Rockwood, K., Blodgett, J.M., Theou, O., Sun, M.H., Feridooni, H.A., Mitnitski, A., Rose, R.A., Godin, J., Gregson, E., and Howlett, S.E. (2017). A Frailty Index Based on Deficit Accumulation Quantifies Mortality Risk in Humans and in Mice. Sci. Rep. *7*, 43068. https://doi.org/10.1038/srep43068.
46. Cardoso, A.L., Fernandes, A., Aguilar-Pimentel, J.A., de Angelis, M.H., Guedes, J.R., Brito, M.A., Ortolano, S., Pani, G., Athanasopoulou, S., Gonos, E.S., et al. (2018). Towards frailty biomarkers: Candidates from genes and pathways regulated in aging and age-related diseases. Ageing Res. Rev. *47*, 214–277. https://doi.org/10.1016/j.arr.2018.07.004.
47. Ingram, D.K., London, E.D., Reynolds, M.A., Waller, S.B., and Goodrick, C.L. (1981). Differential effects of age on motor performance in two mouse strains. Neurobiol. Aging *2*, 221–227.
48. Flood, J.F., and Morley, J.E. (1990). Pharmacological enhancement of long-term memory retention in old mice. J. Gerontol. *45*, 101–104. https://doi.org/10.1093/geronj/45.3.B101.
49. Kyrtata, N., Emsley, H.C.A., Sparasci, O., Parkes, L.M., and Dickie, B.R. (2021). A Systematic Review of Glucose Transport Alterations in Alzheimer's Disease. Front. Neurosci. *15*, 626636. https://doi.org/10.3389/fnins.2021.626636.
50. Götzl, J.K., Brendel, M., Werner, G., Parhizkar, S., Monasor, L.S., Kleinberger, G., Colombo, A., Deussing, M., Wagner, M., Winkelmann, J., et al. (2019). Opposite microglial activation stages upon loss of PGRN or TREM 2 result in reduced cerebral glucose metabolism. EMBO Mol. Med. *11*, e9711. https://doi.org/10.15252/emmm.201809711.
51. Kleinberger, G., Brendel, M., Mracsko, E., Wefers, B., Groeneweg, L., Xiang, X., Focke, C., Deußing, M., Suárez-Calvet, M., Mazaheri, F., et al. (2017). The FTD -like syndrome causing TREM 2 T66M mutation impairs microglia function, brain perfusion, and glucose metabolism. EMBO J. *36*, 1837–1853. https://doi.org/10.15252/embj.201796516.
52. Xiang, X., Wind, K., Wiedemann, T., Blume, T., Shi, Y., Briel, N., Beyer, L., Biechele, G., Eckenweber, F., Zatcepin, A., et al. (2021). Microglial activation states drive glucose uptake and FDG-PET alterations in neurodegenerative diseases. Sci. Transl. Med. *13*, eabe5640. https://doi.org/10.1126/scitranslmed.abe5640.
53. Smith, D., Pernet, A., Hallett, W.A., Bingham, E., Marsden, P.K., and Amiel, S.A. (2003). Lactate: A preferred fuel for human brain metabolism in vivo. J. Cerebr. Blood Flow Metabol. *23*, 658–664. https://doi.org/10.1097/01.WCB.0000063991.19746.11.
54. Campisi, J., Kapahi, P., Lithgow, G.J., Melov, S., Newman, J.C., and Verdin, E. (2019). From discoveries in ageing research to therapeutics for healthy ageing. Nature *571*, 183–192. https://doi.org/10.1038/s41586-019-1365-2.
55. Horvath, S., and Raj, K. (2018). DNA methylation-based biomarkers and the epigenetic clock theory of ageing. Nat. Rev. Genet. *19*, 371–384. https://doi.org/10.1038/s41576-018-0004-3.
56. Lenz, S., and Peterson, J. (2020). It's Time to Act – the Challenges of Alzheimer's and Dementia for Women.
57. Dong, Y., D'Mello, C., Pinsky, W., Lozinski, B.M., Kaushik, D.K., Ghorbani, S., Moezzi, D., Brown, D., Melo, F.C., Zandee, S., et al. (2021). Oxidized phosphatidylcholines found in multiple sclerosis lesions mediate

neurodegeneration and are neutralized by microglia. Nat. Neurosci. *24*, 489–503. https://doi.org/10.1038/s41593-021-00801-z.

58. Lee, S.M., Kim, E.J., Suk, K., and Lee, W.H. (2011). CD300F blocks both MyD88 and TRIF-mediated TLR signaling through activation of Src homology region 2 domain-containing phosphatase 1. J. Immunol. *186*, 6296–6303. https://doi.org/10.4049/jimmunol.1002184.
59. Zhang, Z.D., Milman, S., Lin, J.R., Wierbowski, S., Yu, H., Barzilai, N., Gorbunova, V., Ladiges, W.C., Niedernhofer, L.J., Suh, Y., et al. (2020). Genetics of extreme human longevity to guide drug discovery for healthy ageing. Nat. Metab. *2*, 663–672. https://doi.org/10.1038/s42255-020-0247-0.
60. Shi, Q., Chang, C., Saliba, A., and Bhat, M.A. (2022). Microglial mTOR Activation Upregulates Trem2 and Enhances b-Amyloid Plaque Clearance in the 5XFAD Alzheimer's Disease Model. J. Neurosci. *42*, 5294–5313. https://doi.org/10.1523/JNEUROSCI.2427-21.2022.
61. Marengoni, A., Angleman, S., Melis, R., Mangialasche, F., Karp, A., Garmen, A., Meinow, B., and Fratiglioni, L. (2011). Aging with multimorbidity: A systematic review of the literature. Ageing Res. Rev. *10*, 430–439. https://doi.org/10.1016/j.arr.2011.03.003.
62. Bushnell B. (2014). BBMap: A fast, accurate, splice-aware aligner. https://www.osti.gov/biblio/1241166.
63. Ewels, P., Magnusson, M., Lundin, S., and Käller, M. (2016). MultiQC: Summarize analysis results for multiple tools and samples in a single report. Bioinformatics *32*, 3047–3048.
64. Dobin, A., Davis, C.A., Schlesinger, F., Drenkow, J., Zaleski, C., Jha, S., Batut, P., Chaisson, M., and Gingeras, T.R. (2013). STAR: Ultrafast universal RNA-seq aligner. Bioinformatics *29*, 15–21.
65. Liao, Y., Smyth, G.K., and Shi, W. (2014). featureCounts: An efficient general purpose program for assigning sequence reads to genomic features. Bioinformatics *30*, 923–930.
66. Anders, S., and Huber, W. (2010). Differential expression analysis for sequence count data. Genome Biol *11*, R106.
67. Love, M.I., Huber, W., and Anders, S. (2014). Moderated estimation of fold change and dispersion for RNA-seq data with DESeq2. Genome Biol. *15*, 550.
68. Lê, S., Josse, J., and Husson, F. (2008). FactoMineR: An R package for multivariate analysis. J. Stat. Softw. *25*, 1–18.
69. Kassambara, A. and Mundt, F. (2020) Factoextra: Extract and Visualize the Results of Multivariate Data Analyses. R Package Version 1.0.7. https://cran.r-project.org/web/packages/factoextra/index.html.
70. Wu, T., Hu, E., Xu, S., Chen, M., Guo, P., Dai, Z., Feng, T., Zhou, L., Tang, W., Zhan, L., et al. (2021). clusterProfiler 4.0: A universal enrichment tool for interpreting omics data. Innovation *2*, 100141. https://doi.org/10.1016/j.xinn.2021.100141.
71. Yu, G., Wang, L.G., Han, Y., and He, Q.Y. (2012). ClusterProfiler: An R package for comparing biological themes among gene clusters. OMICS A J. Integr. Biol. *16*, 284–287. https://doi.org/10.1089/omi.2011.0118.
72. Yu, G.. enrichplot: Visualization of Functional Enrichment Result. R package version 1.20.3. https://yulab-smu.top/biomedical-knowledge-mining-book/.
73. Carlson, M. (2019). org.Mm.eg.db: Genome wide annotation for Mouse. R package version 3.8.2.
74. Schlapp, G., Goyeneche, L., Fernández, G., Menchaca, A., and Crispo, M. (2015). Administration of the nonsteroidal anti-inflammatory drug tolfenamic acid at embryo transfer improves maintenance of pregnancy and embryo survival in recipient mice. J. Assist. Reprod. Genet. *32*, 271–275.
75. Dobin, A., Davis, C.A., Schlesinger, F., Drenkow, J., Zaleski, C., Jha, S., Batut, P., Chaisson, M., and Gingeras, T.R. (2013). STAR: Ultrafast universal RNA-seq aligner. Bioinformatics *29*, 15–21.
76. Dobin, A., and Gingeras, T.R. (2016). Optimizing RNA-Seq Mapping with STAR, in Data Mining Techniques for the Life Sciences (New York: Springer), pp. 245–262. https://link.springer.com/protocol/10.1007/978-1-4939-3572-7_13.
77. Zhu, A., Ibrahim, J.G., and Love, M.I. (2019). Heavy-tailed prior distributions for sequence count data: Removing the noise and preserving large differences. Bioinformatics *35*, 2084–2092.
78. Keren-shaul, H., Spinrad, A., Weiner, A., Colonna, M., Schwartz, M., Amit, I., Keren-shaul, H., Spinrad, A., Weiner, A., Matcovitch-natan, O., et al. (2017). A Unique Microglia Type Associated with Restricting Development of Alzheimer's Disease. Cell *169*, 1276–1290.e17.

STAR★METHODS

KEY RESOURCES TABLE

REAGENT or RESOURCE	SOURCE	IDENTIFIER
Antibodies		
Rabbit polyclonal anti-IBA1	Wako	Cat # 019-19741 RRID:AB_839504
Rabbit polyclonal anti-PU1	Cell Signaling Technology	Cat # 2258 RRID:AB_2186909
Brilliant Violet 785™ anti-mouse CD45.2 antibody	BioLegend	Cat# 109839, RRID:AB_2562604
Brilliant Violet 605(TM) anti-mouse/human CD11b	BioLegend	Cat# 101237, RRID:AB_11126744
APC anti-P2RY12	BioLegend	Cat# 848006, RRID:AB_2721469
InVivoPlus anti-mouse CD16/CD32	Bio X Cell	Cat# BE0307, RRID:AB_2736987
Rabbit monoclonal anti-phospho S6 (Ser235/236)	Cell Signaling Technology	Cat # 4858 RRID:AB_916156
Mouse monoclonal anti-S6	Cell Signaling Technology	Cat # 2317 RRID:AB_2238583
Rabbit monoclonal antiphospho- 4E-BP1 (Thr37/46)	Cell Signaling Technology	Cat # 2855 RRID:AB_560835
Rabbit monoclonal anti-4E-BP1	Cell Signaling Technology	Cat # 9644 RRID:AB_2097841
Goat Anti-Rabbit IgG Antibody, Peroxidase Conjugated	Milipore	Cat# AP132P RRID:AB_90264
Anti-actin antibody conjugated to horseradish peroxidase	Merck	Cat # A3854 RRID:AB_262011
Goat anti-mouse conjugated to horseradish peroxidase	Thermo Fisher Scientific	Cat # 31430 RRID:AB_228307
Goat anti-rabbit conjugated to horseradish peroxidase	Thermo Fisher Scientific	Cat # 31460 RRID:AB_228341
Rat anti-mouse CLEC7a/DECTIN1	Novus	Cat # MAB17561 RRID:AB_2081654
Rabbit monoclonal anti-mouse/human NLRP3	Cell Signaling Technology	Cat # 15101T RRID:AB_2722591
Chemicals, peptides, and recombinant proteins		
M16 medium	Sigma Aldrich	Cat #M7292
Embryo tested mineral oil	Sigma Aldrich	Cat # 76235
GeneArt™ CRISPR Nuclease mRNA	Invitrogen	Cat # A29378
Paraformaldehyde	Sigma Aldrich	Cat #P6148
Ethylene glycol	Sigma Aldrich	Cat # 324558
Polyvinylpyrrolidone	Sigma Aldrich	Cat # PVP40
Hematoxylin Solution, Mayer's	Sigma Aldrich	Cat # MHS16
Eosin B	Sigma Aldrich	Cat # 861006
Triton X-100	Sigma Aldrich	Cat #T8787
Fetal Bovine Serum	Invitrogen	Cat # A99835
3,3′-Diaminobenzidine (DAB)	Sigma Aldrich	Cat #D8001
DPX Mountant for histology	Sigma Aldrich	Cat # 06522
TRIzol Reagent	Invitrogen	Cat # A93003
M-MLV reverse transcriptase	Invitrogen	Cat # 28025013
TaqMan Fast Advanced Master Mix	Applied Biosystems	Cat # 4444557
Percoll® PLUS	Sigma Aldrich	Cat # GE17-5445-02
BODIPY™ 493/503 (4,4-Difluoro-1,3,5,7,8-Pentamethyl-4-Bora-3a,4a-Diaza-*s*-Indacene)	Invitrogen	Cat #D3922
DMEM/F-12, GlutaMAX™ supplement	Gibco	Cat # 10565018
Recombinant Mouse M-CSF (carrier-free)	Biolegend	Cat # 576406
Lipopolysaccharides from Escherichia coli O55:B5	Sigma Aldrich	Cat #L2880
L-Glutamine	Sigma Aldrich	Cat #G8540

(*Continued on next page*)

Continued

REAGENT or RESOURCE	SOURCE	IDENTIFIER
Sodium pyruvate	Sigma Aldrich	Cat #P5280
Dextrose	Sigma Aldrich	Cat #D9434
HEPES	Sigma Aldrich	Cat # PHR1428
Oligomycin from Streptomyces diastatochromogenes	Sigma Aldrich	Cat #O4876
Carbonyl cyanide 4-(trifluoromethoxy) phenylhydrazone	Sigma Aldrich	Cat #C2920
Antimycin A from Streptomyces sp.	Sigma Aldrich	Cat # A8674
Rotenone	Sigma Aldrich	Cat #R8875
Bicinchoninic Acid solution	Sigma Aldrich	Cat #B9643
18F-2-fluor-2-desoxi-*d*-glucosa (18F-FDG)	Synthetized in house at CUDIM	N/A
Heparin sodium salt	Sigma Aldrich	Cat #H3149
Rapamycin from Streptomyces hygroscopicus	Sigma Aldrich	Cat #R0395
Bio-Rad Protein Assay Dye Reagent Concentrate	Bio-Rad	Cat #5000006
NuPAGE™ 4 to 12%, Bis-Tris	Invitrogen	Cat # NP0321BOX
NuPAGE ™ MOPS SDS Running buffer	Invitrogen	Cat # NP0001
iBlot2® Transfer Stack	Invitrogen	Cat # IB23002
Restore™ PLUS Western Blot Stripping Buffer	Thermo Fisher Scientific	Cat # 46430
Insulin 2.5cc - 40UI CANINSULIN	MSD Animal Health	N/A
Critical commercial assays		
Direct-zol RNA Miniprep Plus Kits	Zymo Research	Cat #R2070
TruSeq Stranded mRNA LT Sample Prep Kit	Illumina	15031047 Rev. E
LEGENDplex Mouse Inflammation Panel (13-plex)	Biolegend	Cat # 740446
Seahorse XFp FluxPak	Agilent Technologies	Cat # 103022-100
Deposited data		
Raw data RNAseq	This article	Deposited in NCBI (SRA) under accession number SRR21771247-SRR21771254 (PRJNA885873).
Experimental models: Organisms/strains		
C57BL/6J	The Jackson Laboratory	RRID:IMSR_JAX:000664
CD300f knockout mice (CD300f$^{-/-}$)	Xi et al., 2010[13] -Genentech	N/A
CD300f knockout mice (CD300f$^{-/-IPMon}$)	This article	MGI:7525705
B6D2F1	UBAL Facility	N/A
Oligonucleotides		
See Table S6		N/A
Software and algorithms		
ImageJ (Rasband, NIH)	NIH	https://ImageJ.nih.gov/ij/download.html
BBMap	Bushnell, 2014[62]	https://www.osti.gov/biblio/1241166
FastQC v0.11.9	Andrews 2010	http://www.bioinformatics.babraham.ac.uk/projects/fastqc/
MultiQC v1.11	Ewels et al., 2016[63]	https://multiqc.info
STAR 2.7.10a	Dobin et al., 2013[64]	https://github.com/alexdobin/STAR
FeatureCounts v2.0.1	Liao et al., 2014[65]	https://subread.sourceforge.net
DESeq2 v1.36.0	Anders and Huber, 2010[66]; Love et al. 2014[67]	https://bioconductor.org/packages/release/bioc/html/DESeq2.html
FactoMineR v2.4	Lê et al., 2008[68]	https://CRAN.R-project.org/package = FactoMineR

(*Continued on next page*)

Continued

REAGENT or RESOURCE	SOURCE	IDENTIFIER
Factoextra v1.0.7	Kassambara & Mundt, 2020[69]	https://CRAN.R-project.org/package = factoextra
Pheatmap v1.0.12	Kolde 2019	https://CRAN.R-project.org/package = pheatmap
EnhancedVolcano v1.14.0	Blighe et al. 2014	https://github.com/kevinblighe/EnhancedVolcano
ClusterProfiler 3.17	Wu et al. 2021[70] Yu et al. 2012[71]	https://bioconductor.org/packages/clusterProfiler
Enrichplot v1.16.2	Yu 2022[72]	https://bioconductor.org/packages/enrichplot
Org.Mm.e.g.,.db 3.8.2	Carlson 2019[73]	https://bioconductor.org/packages/org.Mm.eg.db
AnyMaze software	Stoelting Co.	https://www.any-maze.com/
PMOD software, v. 3.8	PMOD Technologies, Ltd., Zurich, Switzerland	N/A
Prism 8 software version 8.2.1	GraphPad	https://www.graphpad.com/
Biorender		https://www.biorender.com/
Other		
Accu-Check active glucose strips	Roche	Cat # 06656757

RESOURCE AVAILABILITY

Lead contact

Further information and requests for resources and reagents should be directed to and will be fulfilled by the lead contact, Hugo Peluffo (Hugo.Peluffo@ub.edu).

Materials availability

All unique/stable reagents generated in this study are available from the lead contact with a completed materials transfer agreement.

Data and code availability

- RNA-seq data have been deposited at NCBI and are publicly available as of the date of publication. Accession numbers are listed in the key resources table. Microscopy data reported in this paper will be shared by the lead contact upon request.
- This paper does not report original code.
- Any additional information required to reanalyze the data reported in this paper is available from the lead contact upon request.

EXPERIMENTAL MODEL AND STUDY PARTICIPANT DETAILS

All experimental protocols were approved by the Institutional Animal Ethics Committee (protocol number 014–16, 014-14, 007–18, 021–22), in accordance with national law 18.611 and international animal care guidelines (Guide for the Care and Use of Laboratory Animal). Both male and female mice were used with ages from 6 to 30 month old. The sex and the age of the mice is indicated in the text and figure legends. Mice were housed under SPF conditions on individually ventilated cages (5–6 mice per cage, Tecniplast, Milan, Italy) containing chip bedding (Toplit 6, SAFE, Augy, France), in a controlled environment at 20 ± 1°C with a relative humidity of 40–60%, in a 14/10 h light-dark cycle. Autoclaved food (Labdiet 5K67, PMI Nutrition, IN, US) and autoclaved filtered water were administered *ad libitum*.

Homozygous CD300f knockout mice (CD300f−/− from Genentech, termed CD300f$^{-/-}$ herein) on a C57BL6J (The Jackson Lab, RRID:IMSR_JAX:000664) background were backcrossed to homozygosis two times with the C57BL/6J WT colony of the Institut Pasteur de Montevideo to ensure that WT animals represent proper controls. Mice were housed separated by genotype, except for one cohort. The criteria for animal sacrifice of the aging cohorts were decided by the Laboratory Animal Biotechnology Unit (UBAL) animal facility personnel that were unaware of the genotype and in accordance with their welfare protocols. Intensive monitoring of aged mice was performed to avoid unnecessary suffering and loss of valuable data when mice are found dead. However, excessive censoring of mice can impact aging studies and longevity estimation due to easily observable external non-lethal lesions. To take these two concepts into account, animals were considered to be at the endpoint and euthanized when they showed one or more

clinical signs suggestive of imminent death such as reluctance to move, low body temperature, anorexia, slow or laborious respiration, 20% loss of body weight relative to baseline, ascites, or persistent rectal or uterine prolapses.

A new CD300f knockout mice line was generated (C57BL/6J-Cd300lf<em1Ipmon>/Ipmon, MGI:7525705, termed CD300f$^{-/-IPMon}$ herein). All animal procedures to generate the knock-out line were performed at the SPF animal facility of the UBAL of Institut Pasteur de Montevideo. The CD300f$^{-/-IPMon}$ knockout line was produced using CRISPR/Cas9 system. Cytoplasmic microinjection was performed in C57BL/6J (The Jackson laboratory, RRID:IMSR_JAX:000664) zygotes using a mix of 100 ng/μL GeneArt CRISPR Nuclease mRNA (Invitrogen, Cat # A29378) and 25 ng/μL of each sgRNA (2 guides were used, Figure S7) (Synthego), diluted in standard microinjection buffer. Viable embryos were cultured overnight in M16 medium (Sigma Aldrich, Cat #M7292) microdrops under embryo tested mineral oil (Sigma Aldrich, Cat # 76235), in 5% CO2 in air at 37°C. The next day, 2-cell embryos were transferred into the oviduct of B6D2F1 0.5 days postcoitum pseudopregnant females (20 embryos/female in average), following surgical procedures established in our animal facility. For surgery, recipient females were anesthetized with a mixture of ketamine (110 mg/kg, Pharmaservice, Ripoll Vet, Montevideo, Uruguay) and xylazine (13 mg/kg, Seton 2%; Calier, Montevideo, Uruguay). Tolfenamic acid was administered subcutaneously (1 mg/kg, Tolfedine, Vetoquinol, Madrid, Spain) in order 18 to provide analgesia and anti-inflammatory effects.[74] Pregnancy diagnosis was determined by visual inspection by an experienced animal caretaker two weeks after embryo transfer, and litter size was recorded on day 7 after birth. Pups were tail-biopsied and genotyped 21 days after birth, and mutant animals were maintained as founders. Genetic modification (Figure S7) was confirmed by Sanger sequencing. The CD300f$^{-/-IPMon}$ line was established after producing F4 homozygous animals that were used for experiments.

To obtain data relevant for aging under closer to physiological conditions in non-laboratory animals, one cohort of CD300f−/− (Genentech) mice and one of CD300f$^{-/-IPMon}$ mice were maintained at a specific location of the URBE animal facility of the Faculty of Medicine (UDELAR) which is not specific pathogen free (SPF). Mice were housed on individually non-ventilated cages (5–6 mice per cage, Tecniplast, Milan, Italy), in a controlled environment at 20 ± 1°C with a relative humidity of 40–60%, in a 14/10 h light dark cycle. Autoclaved food (Labdiet 5K67, PMI Nutrition, IN, US) and autoclaved filtered water were administered *ad libitum*. Under these conditions, animals may be infected with *Corynebacterium kutscheri*, *Mycoplasma pulmonis*, Murine hepatitis virus (MHV), Sendai virus (HVJ), Minute virus of mice (MVM), Theiler's murine encephalomyelitis virus (TMEV-GDVII), but are free from endo and ectoparasites and zoonosis.

METHOD DETAILS

Complete blood count

For complete blood counts, blood was drawn from mice (by cardiac puncture using deep anesthesia or from the submandibular vein) and immediately transferred to tubes containing EDTA potassium salts as an anticoagulant and evaluated on an automated analyzer BC-5000Vet (Mindray Medical International Ltd., Shenzhen, China). Among the hematological parameters examined were total white blood cells (WBC) count, lymphocyte count, neutrophils count, monocyte count, basophils count, eosinophil count, red blood cells (RBC) count, hemoglobin (HGB) concentration, hematocrit (HCT) level, mean corpuscular volume (MCV), mean corpuscular hemoglobin (MCH), mean corpuscular hemoglobin concentration (MCHC), platelet (PLT) count and the mean platelet volume (MPV).

Hepatic and renal function

To assess liver and kidney function whole blood from cardiac puncture was analyzed using the Pointcare V2 Chemistry Analyzer (Tianjin MNCHIP Technologies Co., China). The parameters determined were total proteins (TP), albumin (ALB) level, globulin (GLO) level, ALB/GLO ratio, total bilirubin (TBIL) level, alanine aminotransferase (ALT) level, aspartate aminotransferase (AST) level, gamma glutamyl transpeptidase (GGT) level, blood urea nitrogen (BUN) level, creatinine (CRE) level, BUN/CRE ratio and glucose (GLU) level.

Metabolic tests: Glucose tolerance test, pyruvate tolerance test, and insulin tolerance test

Mice subjected to the glucose tolerance test (GTT) were fasted for 12–14 h and injected via i.p. with a dextrose solution (1.5 g/kg, Sigma Aldrich, Cat #D9434). For the pyruvate tolerance test (PTT) and insulin tolerance test (ITT) mice were fasted for 6 h and were injected via i.p. with sodium pyruvate (1.5 g/kg, Sigma Aldrich, Cat #P5280) or insulin (0.5 U/kg, MSD Animal Health, 2.5cc - 40UI CANINSULIN). Blood samples were obtained from the tail at 0, 10, 20, 60 and 120 min after i.p injection and glucose concentration were determined using Accu-Check active glucose strips and a glucometer (Roche, Cat # 06656757).

Histological and immunohistochemistry procedures

Deeply anesthetized mice with ketamine/xylazine were intracardially perfused with ice-cold 4% solution of paraformaldehyde (PFA) (Sigma Aldrich, Cat #P6148) in phosphate buffer and the different tissues and organs were collected. The tissues were postfixed at 4°C in the same fixative for 3–4 h, cryoprotected with a 30% sucrose solution in phosphate buffer for 72 h at 4°C and rapidly frozen in liquid nitrogen and stored at −80°C. Parallel sections of brain (coronal) and liver were obtained using a cryostat (Leica CM1850 UV). Thirty μm-thick sections were either mounted in gelatinized slides or stored as free-floating sections in an antifreeze solution containing 30% sucrose, 30% ethylene glycol and 1% polyvinylpyrrolidone (Sigma Aldrich, Cat # PVP40) in PBS at −20°C. Liver sections

were stained with Mayer's Hematoxylin (Sigma Aldrich, Cat # MHS16) and Eosin (Sigma Aldrich, Cat # 861006). The percentage of infiltrated area in the liver sections was assessed in at least 5 different x4 fields by an observer blinded for the genotype group.

For immunohistochemical staining anti-Iba1 (1:1600, Wako, Cat # 019–19741, RRID:AB_839504), anti-CLEC7a/DECTIN1 (Novus, Cat # MAB17561) and anti-PU1 (1:400, Cell Signaling, Cat # 2258 RRID:AB_2186909) antibodies were used to label microglia and macrophages/monocytes in brain and liver. In all cases, frozen free-floating sections were washed with PBS-1% Triton X-100 (PBS-T) and incubated for 10 min with 2% H2O2 and 70% methanol in PBS solution to block endogenous peroxidase. An antigen retrieval treatment was applied to unmask the PU.1 nuclear antigen by incubating the liver sections in sodium citrate buffer (pH 8.5) for 40 min at 80°C and 20 min at room temperature (RT), previous to the endogenous peroxidase inhibition. Non-specific binding was avoided by incubating the sections for 1 h at RT with blocking buffer (BB) containing 10% fetal bovine serum (FBS) (Invitrogen, Cat # A99835) in PBS-T. The sections were then incubated with the corresponding primary antibody overnight at 4°C. After washing, the sections were incubated for 1 h at room temperature with an anti-mouse antibody conjugated to horseradish peroxidase (Thermo Fisher Scientific, Cat # 31430, RRID:AB_228307) for the CLEC7a antigen and with an anti-rabbit IgG Antibody, Peroxidase Conjugated (Millipore, Cat# AP132P, RRID:AB_90264) for IBA1 and PU1. Following a washing step, the sections were further incubated for 3–5 min with 3,3-diaminobenzidine (Sigma Aldrich, Cat #D8001), washed and mounted in DPX (Sigma Aldrich, Cat # 06522).

RNA extraction and qPCR

Total RNA was isolated from frozen brain, liver, or lung using TRIzol Reagent (Invitrogen, Cat # A93003), and further purified employing the Direct-zol RNA MiniPrep Plus kit (Zymo Research, Cat #R2070) following the manufacturer's protocol. All samples were treated with DNase I. RNA concentrations were quantified using Nanodrop and reversed transcribed using M-MLV reverse transcriptase (Invitrogen, Cat # 28025013) and random primers (Invitrogen, Cat #48190011). Quantitative PCR (qPCR) was performed using Applied Biosystems TaqMan reagents including Fast Advanced Master Mix (Cat # 4444557) and the following probes: *il1β* (Cat # Mm01336189_m1), *il6* (Cat # Mm00446190_m1), *ccl2* (Cat # Mm00441242_m1), *ccl3* (Cat # Mm00441259_g1), *trem2* (Cat # Mm04209424_g1), *cd11c/itgax* (Cat # Mm00498698_m1), *gh* (Cat # Mm00433590_g1), *prl* (Cat # Mm00599950_m1) and *gapdh* (Cat # Mm99999915_g1). The relative gene expression of each sample was determined with the 2-ΔΔCT (Livak) method of analysis. Target genes were normalized to the reference gene *gapdh*. qPCR was performed using the QuantStudio 3 apparatus with the following cycling conditions: 50°C for 2 min, 95°C for 2 min, 40 cycles at 95°C for 1 s and 60°C for 20 s.

RNA sequencing and transcriptomic analysis

For the RNAseq experiment, one brain hemisphere of four CD300f−/− and four WT 30 months old female mice were processed to extract total RNA, as described above. RNA quality was determined in a Bioanalyzer 2100 (Agilent). An RNA Integrity Number (RIN) higher than 8 was considered acceptable to continue to library construction and sequencing, which was carried out at Macrogen (Korea). TruSeq Stranded mRNA LT Sample Prep Kit (Illumina, 15031047 Rev. E) was used for library construction and paired-end reads (150x2 base pairs) were obtained by Illumina sequencing. Raw data were deposited in NCBI (SRA) under accession number SRR21771247-SRR21771254 (PRJNA885873). BBduk[62] was used to trim the reads. Sequence quality of raw and processed reads was assessed with FastQC v0.11.9 (Andrews 2010, http://www.bioinformatics.babraham.ac.uk/projects/fastqc/) and MultiQC v1.11.[63] STAR[75] was used to map the reads to the mouse genome using GRCm39.primary_assembly and Gencode release M25 gene annotations; alignment was performed using standard ENCODE options.[76] Expression counts were obtained at the gene level using FeatureCounts v2.0.1[65] with options -p -s 2 *-M*–fraction. Summary results of read numbers, mapping and gene counts are indicated in Table S2.

Given the obtained read count matrix, the R package DESeq2 v1.36.0 was used to normalize the data, correct for the different sequencing depth of the libraries and to test for differential expression. A minimum pre-filtering of the count matrix was done to keep only those rows that have at least 10 reads. Principal component analyses were performed with the R packages FactoMineR v2.4[68] and factoextra v1.0.7[69] and was based in variance stabilized transformation of data (vst, blind = TRUE) after selection of the 500 top leading genes. To test for differential expression and estimate the log2 fold changes (log2FC) between CD300f−/− and WT genotypes, Wald tests were performed for both the hypothesis |log2FC|>0 and |log2FC|>1. Shrinkage of effect size estimates (log2FC) was done by the apeglm method[77] implemented in DESeq2. For multiple testing correction, we used a stratified false discovery approach, with Benjamini and Hochberg FDR corrected p values. We defined as differentially expressed genes those presenting FDR-corrected p value <0.1 and abs(log2FC corrected by apeglm) > 0.35, a threshold that implies a minimum effect size of about 25%. Expression heatmaps were based on vst data (blind = FALSE) and produced with the R pheatmap v1.0.12 package (Kolde 2019 _pheatmap: Pretty Heatmaps_. R package version 1.0.12, https://CRAN.Rproject.org/package=pheatmap>); for each gene set of interest, only those genes with average expression value above 10 and |apeglm log2FC|>0.35 were included in the heatmap. Volcano plots were produced with the R/Bioconductor package EnhancedVolcano v1.14.0 (Blighe K., Rana S., Lewis M. EnhancedVolcano 2019: publication-ready volcano plots with enhanced coloring and labeling, https://github.com/kevinblighe/EnhancedVolcano). Functional analysis was performed through over-representation analysis (ORA) of KEGG pathways and Gene Ontology (Biological Process domain) terms. Gene set enrichment analysis (GSEA) of particular gene sets was also conducted. The R/Bioconductor packages ClusterProfiler[70,71], enrichplot (Yu G. 2022. enrichplot: Visualization of Functional Enrichment Result. R package version 1.16.2, https://yulab-smu.top/) and org.Mm.e.g.,.db (Carlson M. 2019 Genome wide annotation for Mouse. R package version 3.8.2.) were used for these functional analyses. Gene sets of interest were obtained from the following

sources: ATF4 gene set was kindly provided by Mauro Costa-Matioli; disease associated microglia (DAM) and disease inflammatory macrophages (DIM) gene sets were obtained from[41,78] (broad DAM, conserved DAM, "Keren-Shaul" DAM, broad DIM and conserved DIM); the frailty gene list was obtained from (46); the SenMayo senescence gene signature was obtained from[38]. We also evaluated the lipid-droplet accumulation microglia phenotype using gene lists specified in[42], though no enrichment was found by the GSEA analysis.

Flow cytometry

Mice brains were placed into a Dounce homogenizer with RPMI and thoroughly homogenized. After adding 30% of Percoll PLUS (Sigma Aldrich, Cat # GE17-5445-02), the homogenized samples were centrifuged at 800 g for 15 min. The supernatant was discarded and the pellet was resuspended in FACS buffer (2% FBS in DPBS) and further centrifuged at 800 g for 5 min. Samples were then stained with BODIPY 493/503 (Invitrogen, Cat #D3922) 2M together with an antibody mixture containing brilliant Violet 785 anti-mouse CD45.2 antibody (BioLegend, Cat# 109839, RRID:AB_2562604), brilliant Violet 605(TM) anti-mouse/human CD11b (BioLegend, Cat# 101237, RRID:AB_11126744), APC anti-P2RY12 (BioLegend, Cat# 848006, RRID:AB_2721469) and InVivoPlus anti-mouse CD16/CD32 (Bio X Cell, Cat# BE0307, RRID:AB_2736987) in FACS buffer. All the antibodies were diluted 1/250. Samples were incubated in dark for 15 min at 37°C followed by a wash with FACS buffer. The samples were immediately analyzed using a BD FACSymphony A5 cytometer.

Novel object recognition (NOR)

Mice were placed in a white acrylic chamber (25 × 25 cm base and 35 cm height) over the course of three days during the habituation, familiarization and testing sessions. Before each session, mice were transferred and adapted, for at least 1 h, to the room where behavioral procedures were conducted. On day 1, mice were habituated to the chamber for 5 min. The next day, in the familiarization session, mice were placed in the chamber, for 10 min, with two identical objects laid on the diagonal. On the third day, during the testing session, one of the familiar objects was replaced by a new object. Mice were allowed to explore the objects for 10 min. No preference for the familiar or the novel object was previously verified on a pilot test. The objects and chamber were cleaned before and between sessions with 70% ethanol to remove odor cues. Testing sessions

were recorded using AnyMaze software (Stoelting Co.) and later analyzed by a trained observer blinded to the experimental group. The time exploring each object over a 20 s period of exploration of both objects was analyzed.

Barnes Maze test

The Barnes Maze apparatus and protocol have been previously described[26], and consisted on a white circular acrylic slab (75 cm in diameter and elevated 58 cm above the floor), with twenty holes at regular distances (5 cm in diameter and located 5 cm from the perimeter). A black acrylic escape box (19 × 8 × 7 cm) was placed under one of the holes. Four different spatial cues were located around the maze and remained unaltered throughout the entire test. Before each phase, mice were transferred and adapted, for at least 1 h, to the room where behavioral procedures were conducted. On day one, mice were subjected to a habituation phase in which they were first placed in the escape box for 1 min and later allowed to freely explore the maze for 5 min or until they entered the escape box. There was an interval of at least 1 h before initiating the training phase. The training phase consisted of two sessions in which the mice was placed in one of the quadrants of the maze and allowed to freely explore the apparatus until they entered the escape box or after 3 min had elapsed. The training sessions (2 per day) were conducted for four consecutive days. The maze was cleaned between the sessions with 70% ethanol. Three days after the final training day (Day 7), mice underwent a 1 min probe trial in which the escape box was removed from the apparatus. During the trial sessions and probe trial the time latency to encounter the escape box was recorded.

Parallel rod floor test (ataxia)

Mice in their home cages were placed for 30 min in the behavior testing room for

habituation to the new environment. After habituation, mice were placed in the parallel rod floor apparatus (Stoelting Co.) coupled to the ANY-maze Software for animal tracking. This apparatus consists of a clear acrylic chamber enclosure (20 cm × 20 cm x 30 cm height) with a floor consisting of 1.6-mm diameter rods that are spaced 6.5 mm apart and elevated 1.2 cm above a metal plate. The computer records a foot fault when the mouse's paw slips through the parallel rods and contacts the metal plate closing the circuit. The mice are placed in the apparatus and are allowed to freely explore for 10 min in the absence of the researcher. The apparatus was cleaned with 70% ethanol before continuing with the next mouse.

Bone marrow derived macrophages cultures

Bone marrow derived macrophages (BMDM) were isolated from adult female and male WT and CD300f$^{-/-}$ mice as previously described elsewhere. Briefly, bone marrow was flushed from the femur and tibia with DMEM/F12 (Gibco, Cat # 10565018) supplemented with Penicillin/Streptomycin and 10% FBS (complete DMEM/F12). Cells were plated on to 100 mm bacteriological Petri dish with complete DMEM/F12 and 20 ng/mL recombinant mouse macrophage colony stimulating factor protein (M-CSF) (Biolegend, Cat #576406). On day 4, cells were subcultured in XFe24 plates at 100,000 cells per well or at 200.000 cells per well in XFe96 plates.

Measurement of oxygen consumption rates

Oxygen consumption rates (OCR) and extracellular acidification rates (ECAR) were determined using Seahorse XFe24 extracellular flux analyzer (Agilent Technologies) for initial female cell cultures, or Seahorse XFe Pro 96 for experiments comparing male and female cells. BMDM seeded on XFe24 plates were pretreated for 18 h with 100 ng/mL Lipopolysaccharide (LPS) (Sigma Aldrich, Cat #L2880) in complete DMEM/F12 and 5 ng/mL M-CSF. Prior to the metabolic measurements, cells were incubated for 1 h with Seahorse media (DMEM supplemented with 1 mM sodium pyruvate, 5 mM glucose, 2 mM glutamine, 5 mM HEPES, pH 7.4), in a stove at 37°C without CO2. Following the initial basal measurements, successive measurements were then made after the sequential addition of 2.5 μM oligomycin (Sigma Aldrich, Cat #O4876), 2 μM carbonyl cyanide- 4-(trifluoromethoxy) phenylhydrazine (FCCP) (Sigma Aldrich, Cat #C2920) (two 1 μM additions), and a mixture of 2.5μM antimycin (AA) (Sigma Aldrich, Cat # A8674) and 2.5 μM rotenone (Rot) (Sigma Aldrich, Cat #R8875). After each assay, the protein content of each well was determined with the bicinchoninic acid (BCA) assay and the OCR and ECAR were normalized to the protein content. The non-mitochondrial respiration (AA/Rot-resistant respiration) was subtracted from all the OCR. Maximum oxygen consumption rate (or maximum respiration rate) was determined after the addition of FCCP, and spare respiratory capacity was calculated as the difference between the maximum and basal OCR. ATP-independent respiration was determined after the addition of oligomycin. ATP-dependent respiration was calculated subtracting the ATP-independent respiration from the basal oxygen consumption rate.

Western blotting

BMDM cultures were incubated with 20 ng/mL MCSF alone or in addition with LPS (Sigma Aldrich, Cat #L2880) 100 ng/mL for 12 h or with Rapamycin 100 μM (Sigma Aldrich, Cat #R0395) for 1.5 h in DMEM/F12 media. An additional group was generated by incubation in low MSCF (5 ng/mL) for 12 h. Whole-cell extracts were lysed and centrifuged at 14,000 × g to remove cell debris and protein concentration was measured using Bradford reagent (Bio-Rad, Cat #5000006), following the manufacturer's instructions. Samples (15–20 μg) were mixed with loading buffer and resolved in 4–12% polyacrylamide gels (NuPAGETM NovexTM 4–12% Bis-Tris) (Invitrogen, Cat # NP0321BOX) using the NuPAGE TM MOPS SDS Running buffer (Invitrogen, Cat # NP0001). The transference to a nitrocellulose membrane was performed using iBlot2 Transfer Stack supports (Invitrogen, Cat # IB23002).

The following primary antibodies were used (1:1,000 if not stated otherwise): rabbit monoclonal anti-phospho S6 (Ser235/236) (Cell Signaling Technology, Cat # 4858, RRID:AB_916156), mouse monoclonal anti-S6 (Cell Signaling Technology, Cat # 2317, RRID:AB_2238583), rabbit monoclonal antiphospho-4E-BP1 (Thr37/46) (Cell Signaling Technology, Cat # 2855, RRID:AB_560835), rabbit monoclonal anti-NLRP3 (Cell Signaling Technology, Cat # 15101T) and rabbit monoclonal anti-4E-BP1 (Cell Signaling Technology, Cat # 9644, RRID:AB_2097841). Membranes were incubated with the antibodies for 16 h at 4°C in agitation. Anti-actin antibody conjugated to horseradish peroxidase (1:100,000), (Merck, Cat # A3854, RRID:AB_262011) was incubated for 30 min at RT and used as loading control. Anti-mouse and anti-rabbit secondary antibodies produced in goat and conjugated to horseradish peroxidase (1:10,000) (Thermo Fisher Scientific, Cat # 31430, RRID:AB_228307 and Cat # 31460, RRID:AB_228341 respectively) were incubated for 1h at RT. Chemiluminescent images were acquired using a Chemidoc imager (BioRad) and quantified by computer-assisted densitometric analysis (ImageJ). To remove the signals and allow the incubation with other antibodies the Restore PLUS Western Blot Stripping Buffer (Thermo Fisher Scientific, Cat # 46430) was used.

PET/CT imaging

Brain glucose uptake was evaluated by *in vivo* imaging using positron emission tomography/computed tomography (PET/CT) scans with 18F-2-fluor-2-desoxi-*d*-glucosa (18F-FDG) as radiotracer. The study was performed in the Centro Uruguayo de Imagenología Molecular (CUDIM). A nanoScan PET/CT Mediso Preclinical Imaging system based on LYSO scintillators for small animal PET imaging was used. This scanner has a spatial resolution of 0.9 mm and a transaxial field of view (FOV) of 8.0 cm. The data were acquired in list mode in a 212 × 212 × 235 matrix with a pixel size of 0.4 × 0.4 × 0.4 mm and a coincidence window width of 1.0 nsec. The animals were anesthetized with 2% isoflurane in an oxygen flow of 2 L/min, placed in prone position on the scanner bed, and injected i.v. via the caudal vein tail with 100–200 μL of 18F-FDG (25.67 ± 6.09 MBq). PET images (static studies) acquisition started 20 min after radiotracer administration and performed over 30 min. Sinograms were reconstructed using 3D maximum likelihood expectation maximization (MLEM) with 4 iterations and 6 subsets. Semiquantitative analysis was done using PMOD software, v. 3.8 (PMOD Technologies, Ltd., Zurich, Switzerland). PET studies were co-registered with the corresponding CT scan studies for anatomical localization. The images were displayed as coronal, sagittal and axial slices. Using the PFUS module, the brain images were spatially normalized to the mouse brain magnetic resonance imaging (MRI) template included in the PMOD software, to scale the images to the Paxinos and Watson coordinate system (Paxinos and Watson, 1998). The images were previously masked to exclude extracerebral activity and enhance the normalization data. The inverse mathematical transformation was estimated and applied to the volumes-of-interest (VOIs) included in the PMOD mouse brain atlas to fit the VOIs for each animal. The average activity per volume unit (kBq/cc) was subsequently corrected for injected radioactivity and mouse weight and expressed in standardized uptake value (SUV) units. Different VOIs representing brain areas were selected for further evaluation.

QUANTIFICATION AND STATISTICAL ANALYSIS

Continuous variables were evaluated using Student's two-tailed t test, one-way analysis of variance (ANOVA), or two-way ANOVA for repeated measures followed by Sidak's post hoc test, as appropriate. ANOVA followed by Tukey's post-hoc analysis was used for experimental data with more than two experimental groups and normal distribution. For qPCR analysis, non-parametrical Mann-Whitney test was used. Statistical analyses were performed with the Prism 8 software (version 8.2.1) and data were presented as mean ± SEM, considering $p < 0.05$ as statistically significant. Figures were created with BioRender.